Report No. DOT-TST-77-76

USING CROSS-BOREHOLE ELECTROMAGNETIC PROBING TO LOCATE A TUNNEL

Final Report

January 1977

Prepared for the

U.S. DEPARTMENT OF TRANSPORTATION
Office of the Secretary
Washington, D.C. 20590

Technical Report Documentation Page

1. Report No.	2. Government Accession No.	3. Recipient's Catalog No.
DOT-TST-77-76		

4. Title and Subtitle	5. Report Date
USING CROSS-BOREHOLE ELECTROMAGNETIC PROBING TO LOCATE A TUNNEL	January 1977
	6. Performing Organization Code
	8. Performing Organization Report No.
7. Author(s) R. J. Lytle, D. L. Lager, E. F. Laine, and D. T. Davis	
9. Performing Organization Name and Address	10. Work Unit No. (TRAIS)
Lawrence Livermore Laboratory University of California, P.O. Box 808 Livermore, California 94550	11. Contract or Grant No. AS-60048
	13. Type of Report and Period Covered Final Report
12. Sponsoring Agency Name and Address Office of the Secretary U.S. Department of Transportation Washington, D.C. 20590	14. Sponsoring Agency Code TST-45

15. Supplementary Notes

16. Abstract

Experiments were made around a tunnel near Gold Hill, Colorado. The tunnel was horizontally and vertically located within three feet by the earth probing radar system described herein.

Theoretical and experimental studies of electromagnetic interaction with the tunnel found that signal minima can be used to detect and locate the tunnel. These signal minima are found on the transmission side of the tunnel, the side opposite the signal transmitter. No useful variation was found on the reflection side -- the same side as the transmitter. From the appearance of the signal and comparison with Fresnel diffraction, the main mechanism of signal interaction with the tunnel seems to be diffraction rather than refraction or reflection. The signal is appreciably affected by tunnel shape and the presence of back-fill, but not by a metal screen in the tunnel. The best results were obtained at a frequency of 57MHz, giving a wavelength in the ambient medium about equal to the tunnel's radius.

17. Key Words	18. Distribution Statement
Tunneling, site exploration, ground probing radar, electromagnetic (EM) probes, reconstruction algorithms	Document is available to the U.S. Public through the National Technical Information Service, Springfield, Virginia 22161

19. Security Classif. (of this report)	20. Security Classif. (of this page)	21. No. of Pages	22. Price
UNCLASSIFIED	UNCLASSIFIED	41	

01215

USING CROSS-BOREHOLE ELECTROMAGNETIC PROBING TO LOCATE A TUNNEL

R. J. Lytle, D. L. Lager, E. F. Laine, and D. T. Davis

Contents

USING CROSS-BOREHOLE ELECTROMAGNETIC PROBING TO LOCATE A TUNNEL

Abstract

Theoretical and experimental studies of electromagnetic interaction with a tunnel found that signal minima can be used to detect and locate the tunnel. These minima are found on the transmission side of the tunnel, the side opposite the signal transmitter. No useful variation was found on the reflection side — the same side as the transmitter. From the appearance of the signal and comparison with Fresnel diffraction, the main mechanism of signal interaction with the tunnel seems to be diffraction rather than refraction or reflection. The signal is appreciably affected by tunnel shape and the presence of back-fill, but not by a metal screen in the tunnel. The best results were obtained at a frequency of 57MHz, giving a wavelength in the ambient medium about equal to the tunnel's radius. Experiments were made around a tunnel near Gold Hill, Colorado. The tunnel was horizontally and vertically located within three feet.

Introduction

Determining the structure of the earth is of great interest in the search for minerals. In tunneling, knowledge of the location[1] of water or gas pockets or abandoned tunnels[2] can save lives. In excavation projects, equipment can be more conveniently scheduled if the subsurface structure is known in advance.

Recently, workers have better determined a subsurface electromagnetic profile by using reconstruction-technique algorithms[3,4] to interpret the hole-to-hole transmissions of high frequency signals. This technique works quite well when the subsurface region of interest is relatively homogeneous, is not very lossy, and there is a small electrical contrast between the ambient medium and an anomaly of interest. An example of a problem that fits these criteria was determining the extent of fractures induced in a coal seam by detonation of high explosives.[5] The dominant physical mechanism of propagation from transmitter to receiver through this fractured coal medium was easily and adequately described by straight line ray optics.

However, a large electrical contrast between the ambient medium and the anomaly of interest may mean that propagation of the signals is not always governed by ray optics (refraction or reflection).

Such a situation can occur when one electromagnetically probes between drill holes to determine the possible presence and location of a tunnel or cavity. If the size of the anomaly is more than 1/4 of the probing signal's wavelength in the medium, the fields near the anomaly can be adequately described by diffraction. We concentrate herein on a tunnel anomaly, as this is a relatively easy problem to study theoretically and experimentally. Many of the conclusions presented can be extended to apply in a qualitative sense to other high electrical contrast anomalies.

The data interpretation method developed and presented herein is particularly attractive, as with it one can easily and rapidly interpret data in the field. That is, neither a large scientific computer nor even a small hand calculator is required for determination of the tunnel location. All that are required are: successful transmission, a record of the variation of signal intensity with depth for a number of fixed source/receiver orientations, a ruler, a pen, and graph paper.

Theoretical Studies of Electromagnetic Field Variation

ASSUMPTIONS AND SIMPLIFICATIONS IN THE THEORETICAL MODEL

By concentrating on a tunnel as an anomaly, we can consider the simple theoretical problem of an air-filled tunnel of infinite length, or effectively, a tunnel whose ends or bends are far enough removed that their effect on the local electromagnetic field is not observable.

The effect of tunnel shape on the electromagnetic field was considered to be of possible significance. Thus, we have considered interaction with tunnels shaped as right circular cylinders (which yield to an exact mathematical solution in terms of sums of Bessel functions — see Appendix A), and tunnels of arbitrary shape (which can be adequately modeled by an approximate integral-equation approach — see Appendix B).

One method of electronically probing the ground to detect and locate an anomaly is to propagate a signal between two drill holes (see

Fig. 1). If there is a significant anomaly between the two drill holes, then the received signal would hopefully be interpretable such that the location of the anomaly is evident. If the anomaly is not of high electrical contrast with the ambient medium, one can sometimes locate the anomaly by interpreting either seismic[6] or electromagnetic[5,7] propagation data. This report discusses how to locate anomalies that have a high contrast relative to the ambient medium. Most of our attention is directed to electromagnetic probing. The basic experiment modeled in this section consists of physically and electrically small electric dipole transmitters and receivers oriented vertically in a drill hole (i.e., parallel to the axis of the hole). Loop antennas could also be used in the holes, but so far we have seen no need for them.

For convenience, the tunnels of interest are assumed to run approximately parallel to the surface of the earth. We also assume that the drill holes and tunnel are deep enough that electromagnetic interaction with the surface of the earth is negligible. Thus, the actual physical situation is approximately modeled by a point source and point receiver in the presence of an infinitely long tunnel of arbitrary cross section located in an ambient medium of infinite extent.

It is computationally time consuming to calculate the Sommerfeld integrals governing the near field interaction of a point source with an infinitely long tunnel. Thus, we simplify the problem even further by considering line sources rather than point sources. This eliminates the need for computing the Sommerfeld integrals. We have thereby approximated the three dimensional experiment with a two dimensional theoretical model.

A line magnetic current source oriented parallel to the tunnel axis

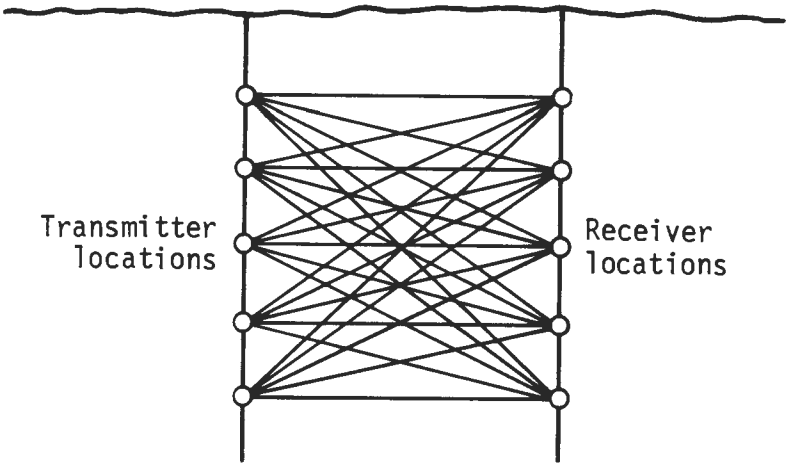

Fig. 1. Subsurface can be effectively sampled through use of multiple transmitter and receiver locations.

generates a field polarized similar to the field from the actual electric dipole source oriented vertically in a drill hole. This polarization is described as transverse electric (TE) relative to the tunnel axis. Many of our calculations have been concerned with the TE excitation. Because of possible interest, we have also computed some fields for a line electric current source oriented parallel to the tunnel axis. This source creates a polarization described as transverse magnetic (TM) relative to the tunnel axis. The TM fields would be qualitatively similar to experimental results obtained with vertically oriented magnetic dipole source and receiver (i.e., loop antennas that have their planes perpendicular to the axis of the drill holes).

Because of the number of assumptions made to simplify the theoretical model and the resultant computations, one should only expect qualitative correlation between theory and experiment, and not an exact quantitative correlation. However, the qualitative assessments of theory and experiment agree surprisingly well, as demonstrated later in this report.

Previous studies of the interaction of electromagnetic waves with infinitely long cylinders have used both exact approaches (for right circular cyclinders)[8-12] and approximate approaches (for cylinders of arbitrary cross section).[13-16] We have used the formulas and insights of these references for this particular application. No new theoretical formulas have been derived. An abbreviated list of the exact formulas used is given in Appendix A. The choice of which approximate method to use was somewhat arbitrary; we chose an integral equation technique,[13,14] given in Appendix B.

CALCULATED VARIATION WITH RIGHT CIRCULAR TUNNELS

To better understand the wave interaction with the tunnel, we solved the boundary value problems for the fields shown in Fig. 2. These idealized models approximate the main details of the antenna/tunnel interaction. The model of Fig. 2 was considered to see if any unusual effects would be encountered if both the transmitter and receiver were near the tunnel. Other calculations were run for the model of Fig. 3, where the transmitter is a large distance from the tunnel, and essentially a plane wave interacts with the tunnel. The first situation studied is depicted in Fig. 4. This model was tested with signals of frequency 57 MHz. The locations of

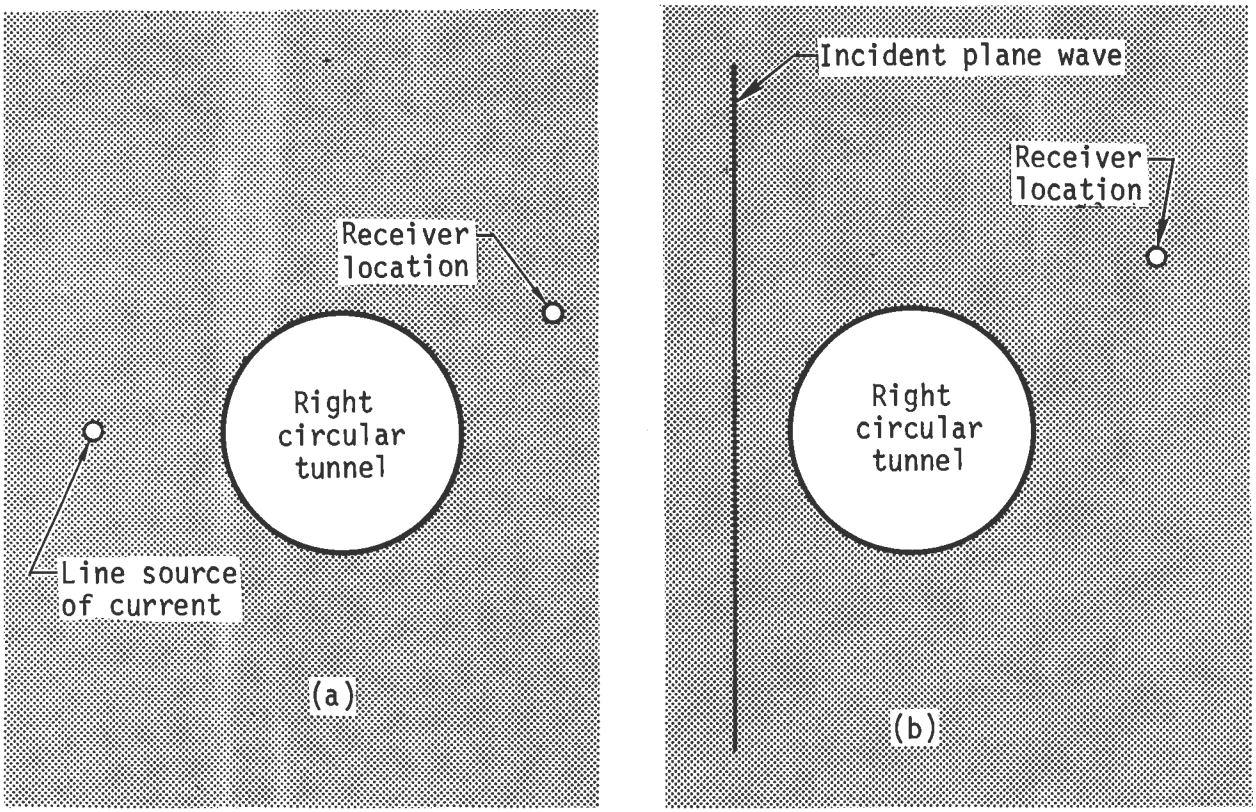

Fig. 2. Experiment was modeled with the actual tunnel approximated by a circular tunnel of radius 4 ft. The excitation considered was either a line source of current (a) or a plane wave (b).

both the transmitter and receiver are close to the edge of the tunnel.

Figure 4a depicts the theoretical prediction for the variation of received signal as the transmitter and receiver are lowered in unison down their drill holes past the tunnel. This is the predicted variation when the electric field is polarized parallel to the drill holes (i.e., as in a TE mode such as occurred in the actual experiments). Note the apparent diffraction effect (an oscillating signal decaying with distance from the top and the bottom of the tunnel) and the sharp minima and maxima in the near vicinity of the tunnel. Calculations show that the sharpest minima can be used as a diagnostic of the tunnel location. As will be seen later, the variation of signal from a line source shown in Fig. 4a is similar to that observed when the excitation is a plane wave (Fig. 2b).

The equations governing the propagation of the longitudinal or compressional component (P wave) of acoustic waves interacting with a tunnel are similar in form to the equations describing the electromagnetic interaction with the tunnel

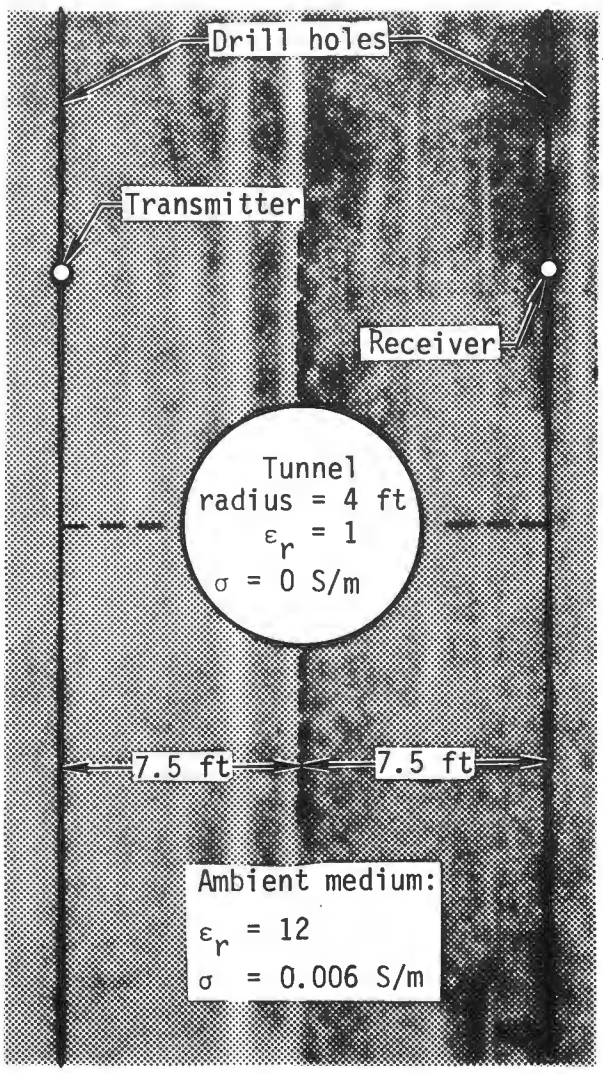

Fig. 3. In the theoretical model, transmitter and receiver, at the same depth, are lowered in unison past the tunnel.

when the electric field is polarized parallel to the drill holes.[17] The only difference in the equations is the propagation constants. One equation is expressed in terms of the acoustic propagation constant k_{ac} and the other is expressed in terms of the electromagnetic propagation constant k_{em}. The difference in estimated nominal propagation velocities v in a hard rock medium such as at Gold Hill, Colorado ($v_{em} \cong 8.6 \times 10^7$ m/s and $V_{ac} \cong 2.7 \times 10^3$ m/s), means that the electromagnetic response at 57 MHz is analogous to the acoustic response at 1800 Hz.

The theoretical electromagnetic response when the magnetic field polarization is perpendicular rather than parallel to the tunnel axis is given in Fig. 4b. This is not the orientation we used in experiments at Gold Hill, but one could use this orientation if loop antennas rather than dipole antennas were used. Note the sharp maxima in the vicinity of the tunnel and the deep minima near the tunnel.

The next theoretical case we considered was for the configuration shown in Fig. 5. For this case, the difference in depth of the transmitter and receiver was fixed at 10 ft, and the transmitter and receiver were lowered in unison past the tunnel. We used a similar method in collecting experimental data at Gold Hill. Figure 6 shows the theoretical receiver response when the data is collected in this way. Note the maxima and minima are offset relative to the center of the tunnel, but the signal shows the same characteristic variation as in Fig. 5.

By referring to Fig. 7, which takes into account the constant 10-ft

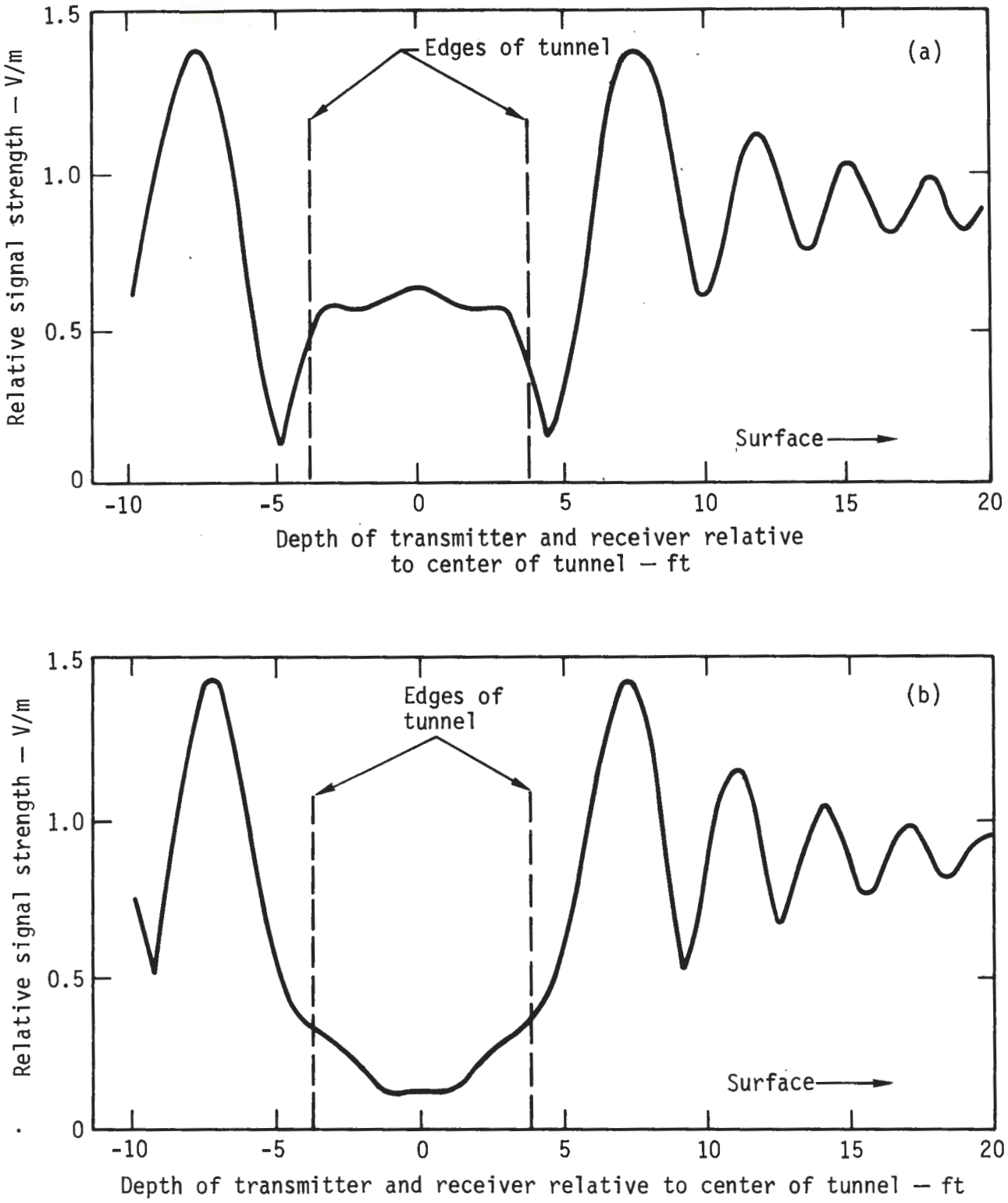

Fig. 4. For the configuration shown in Fig. 3, with the electric field polarized parallel to the drill holes (a) and with the magnetic field polarized parallel to the drill holes (b), the modeled response is an apparent diffraction pattern.

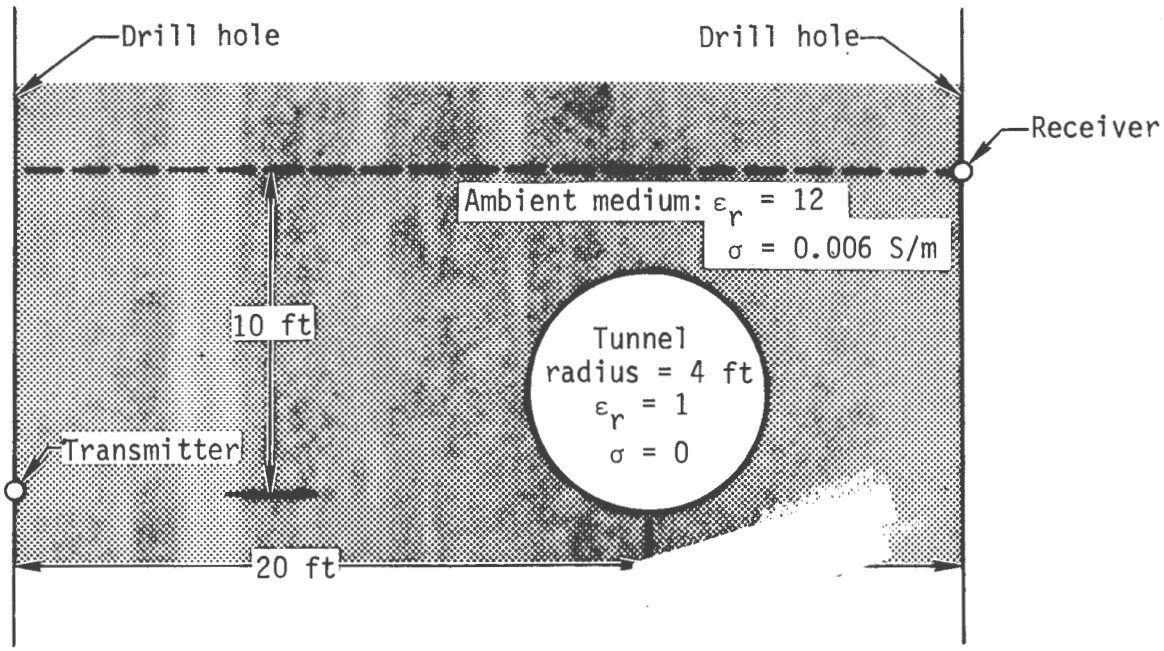

Fig. 5. Modeled transmitter and receiver, separated vertically by ten feet, are lowered in unison past the tunnel.

vertical separation between transmitter and receiver, we see that the signal minima in Fig. 6 are centered about the projected middle of the tunnel. This implies a useful diagnostic. By noting the two strongest adjacent signal minima when sampling in a drill hole and by knowing the constant separation distance between transmitter and receiver, one can define a sector containing the tunnel. The tunnel should lie between two lines originating at the positions where the minima were received. These lines are inclined at an angle θ defined by the horizontal distance D between the transmitter and receiver hole and the vertical separation H between transmitter and receiver [i.e., $\theta = \tan^{-1}(H/D)$].

The variation of signal strength with depth for a fixed difference in depth between transmitter and receiver is what we call a view. By recording data for a number of views, the location of the tunnel can be inferred. (See Fig. 8.) This is the approach we used to interpret our experimental data. It is a modification of a technique known as back projection used in medical diagnostics.

We have generated additional theoretical results to help us understand the complete field behavior. The remainder of the theoretical results for a circular

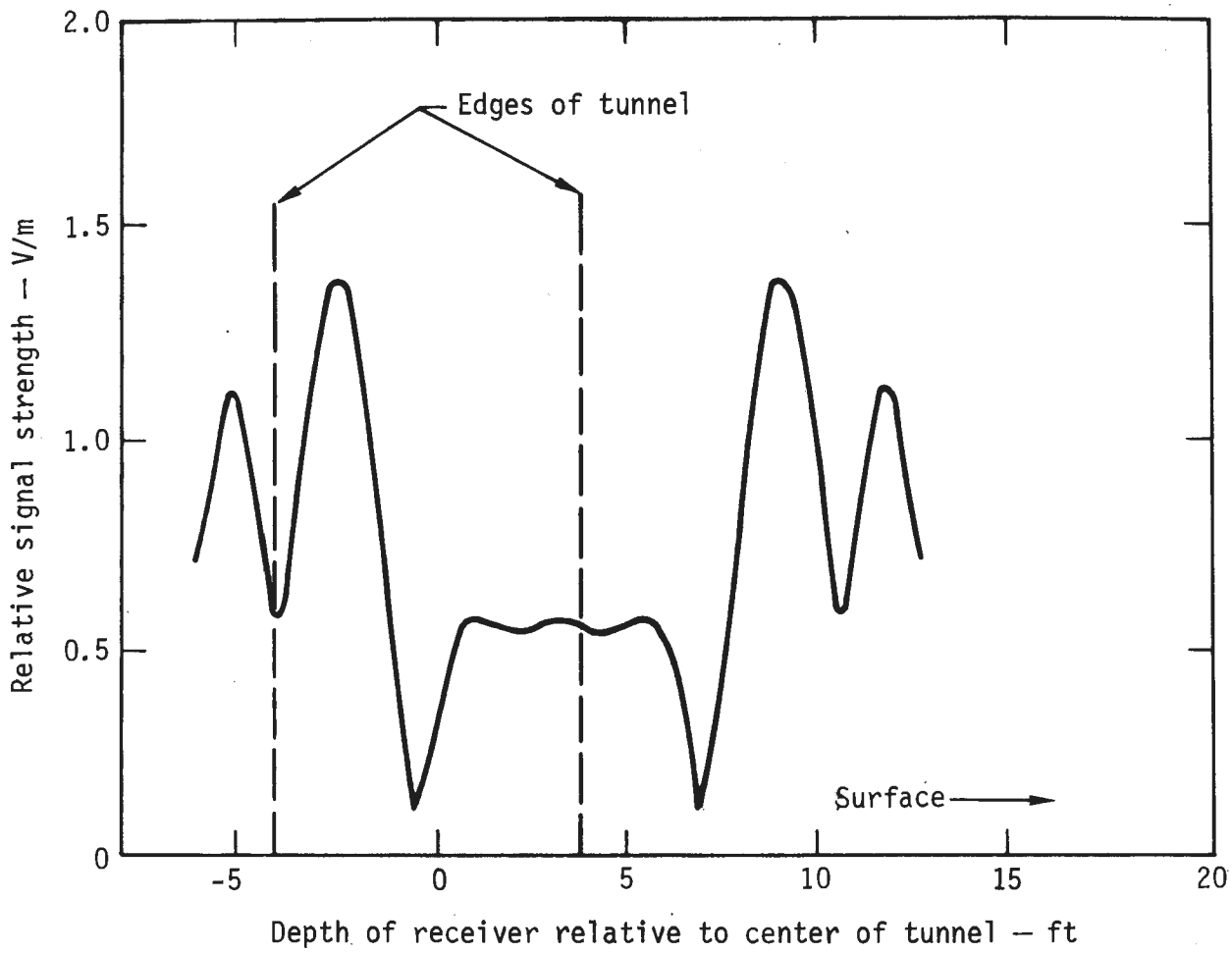

Fig. 6. For the configuration shown in Fig. 5, with the electric field polarized parallel to the drill holes, the modeled response is an apparent diffraction pattern.

tunnel are for the situation of Fig. 3, where a plane wave is incident on the tunnel. The modeled receiver location has been moved about the tunnel for this excitation. This has been done to calculate the signal on both the reflection side and transmission side of the tunnel.

Figure 9 depicts the field strength variation about the tunnel for various frequencies of a TE plane wave incident from the right: Fig. 9a — 80 MHz, Fig. 9b — 57 MHz, Fig. 9c — 25 MHz. The values along any vertical line approximate the data in a drill hole. Due to the volumes of theoretical data generated, the data has been displayed as shading. The darkest color denotes the most intense signal. The gray levels between the maximum and minimum signals were assigned in a linear

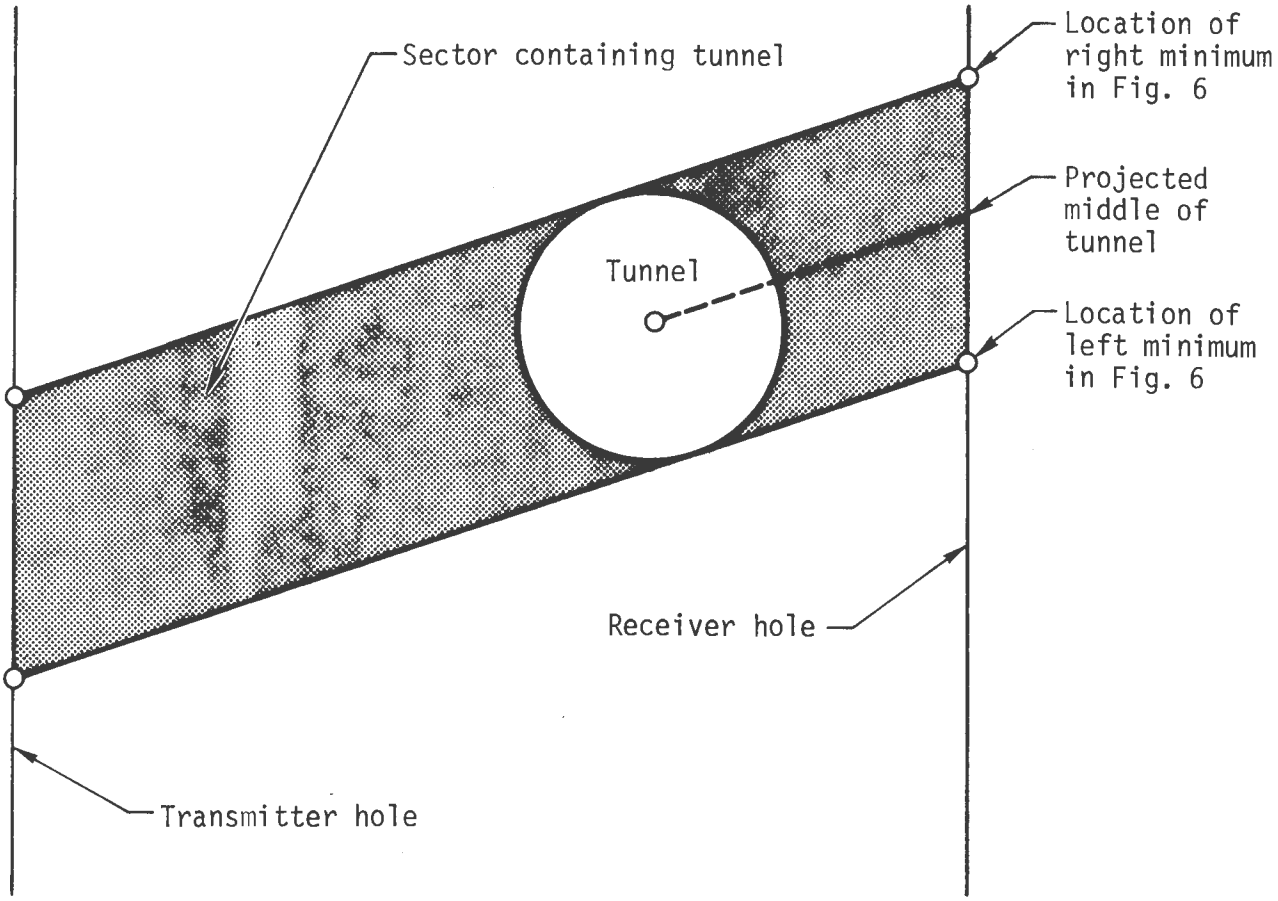

Fig. 7. For a ten-foot offset between transmitter and receiver, the location of the minima of Fig. 6 defines a sector containing the tunnel.

fashion. This theoretical data has given us a better intuition about the diffraction due to a tunnel.

From Fig. 9, the effect of frequency seems to be most evident in the width between successive maxima and minima. The higher the frequency, the more signal variation within a drill hole (which would be a vertical line in these figures). The 57-MHz figure appears to be sufficiently detailed that views can be accurately used to locate the tunnel. Going to a higher frequency gives better detail but may not be required. The lower the frequency, the farther the signal propagates. Thus, the lowest frequency that gives sufficient detail is preferred. The 25 MHz picture does not have enough change in signal level to enable confident interpretation of the presence of a tunnel when there is also small scale geologic noise.

An interesting effect in Fig. 9 is that the presence of the tunnel is not as evident on the reflection side (right side in the figures)

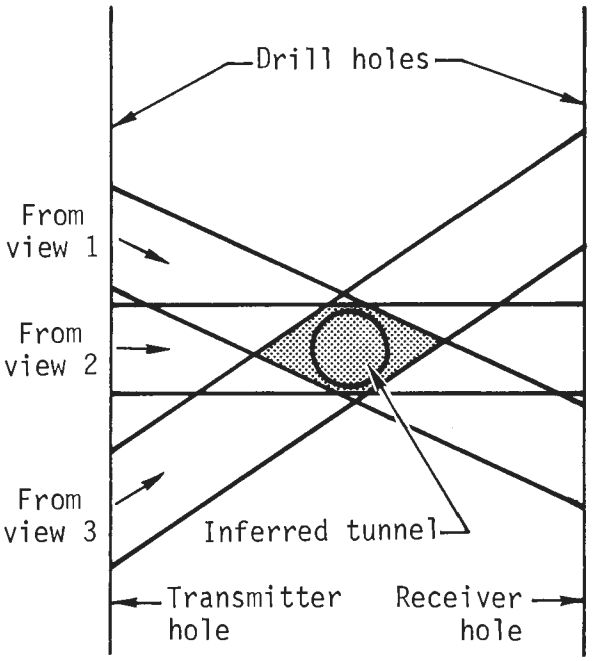

Fig. 8. The superposition of back projections from several views defines the tunnel location.

of the tunnel as on the transmission side. We also observed this experimentally at Gold Hill, but we did not investigate this aspect much further.

One last illustration of TE polarized wave is included (Fig. 10) to show the effect of the plane wave's angle of incidence. The picture shows the result of a plane wave incident from 45° above the right horizontal position. Note the 45° shift of the diffraction pattern about the cylinder (compared to Fig. 9b). This shift enables one to use the "view" concept for relatively small departures of the angle of incidence from horizontal.

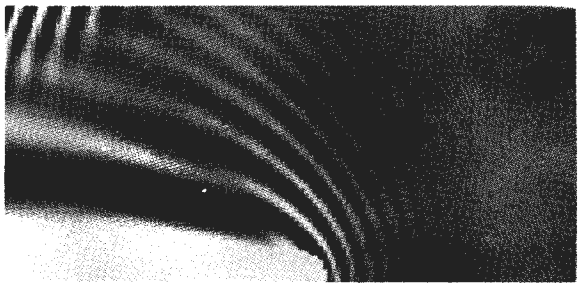

(a) 80-MHz excitation. The manifestation in the upper left is a mathematical artifact due to problems in accurately computing the Bessel function.

(c) 25-MHz excitation.

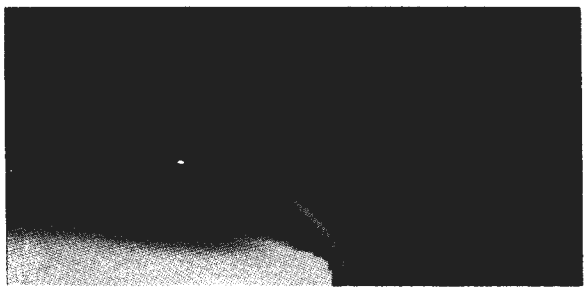

(b) 57-MHz excitation.

Fig. 9. The total field exterior to a right circular tunnel excited by a plane wave incident from the right. Only the upper halves of the tunnel and the field are shown, as the fields are vertically symmetric about the middle of the tunnel. The horizontal axis extends 30 feet to either side of the tunnel. The vertical axis extends from the center of the tunnel to 30 feet. above. The field is TE polarized.

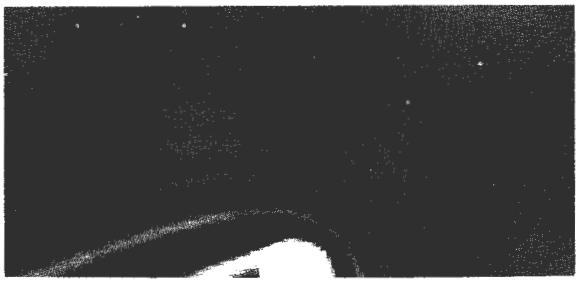

(a) TM polarization.

(b) TE polarization.

Fig. 10. Total field exterior to a right circular tunnel excited by a plane wave incident from 45° above the right horizontal. Only the upper half of the tunnel and the fields are shown. The horizontal axis extends 30 feet to either side of the tunnel. The vertical axis extends from the center of the tunnel to 30 feet above it. The frequency of excitation is 57 MHz.
(a) TM polarization.
(b) TE polarization.

Figure 11 shows the effect a different polarization of the incident signal has on the diffraction pattern. These figures depict the variation of field strength about the tunnel for a TM plane wave incident from the right. Different frequencies of excitation are indicated: Fig. 11a — 80 MHz, Fig. 11b — 57 MHz, Fig. 11c — 25 MHz. Comparing Fig. 11 with Fig. 9 shows the overall effect of using a TM rather than TE incident signal to sense the tunnel is that the signal minima and maxima are shifted in location, but the general character

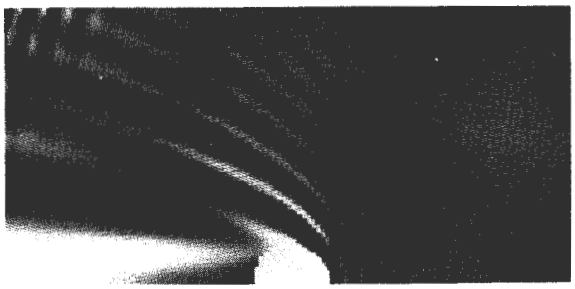

(a) 80-MHz excitation. The manifestation in the upper left is a mathematical artifact due to problems in accurately computing the Bessel function.

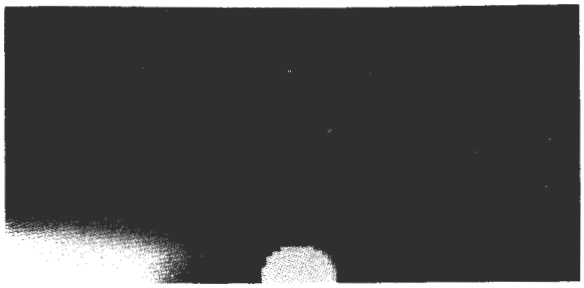

(c) 25-MHz excitation.

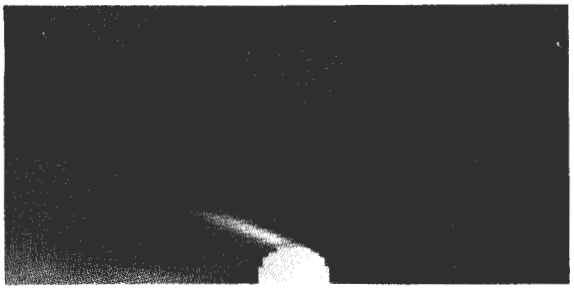

(b) 57-MHz excitation.

Fig. 11. Total field exterior to a right circular tunnel excited by a plane wave incident from the right. Only the upper halves of the tunnel and the field are shown, as the fields are vertically symmetric about the middle of the tunnel. The horizontal axis extends 30 feet to either side of the tunnel. The vertical axis extends from the center of the tunnel to 30 feet above it. The field is TM polarized.

of the view is not significantly different.

These theoretical studies gave us a good "intuitive feel" (after eliminating a number of our misconceptions) for the variation about a tunnel of a signal due to an incident electromagnetic wave. The signal appears to be dominated in the near vicinity of the tunnel by the superposition of the incident signal and a wave diffracted from the top and bottom edges of the tunnel. Note, however, that the effect of the tunnel is strongest close to the tunnel and decays with distance from the tunnel. The quasi-periodic nature of the maxima and minima centered about the tunnel enables one to use simplified back projection to locate the tunnel.

It is of some interest to depict the field strength variation and polarization inside the tunnel. This is not of immediate use in "finding a tunnel", but it does lend itself to giving the reader a more complete understanding of how the electromagnetic wave interacts with a tunnel.[12] For example, by using the results in Fig. 12, one can visualize the induced polarization currents in the tunnel. These polarization currents are the basis of the approximate approach (see Appendix B) used to calculate the fields for more realistic tunnel shapes. The polarization of the induced field, which is perpendicular to the power flow designated by the Poynting vector, is shown in Fig. 13.

CALCULATED VARIATION WITH REALISTICALLY SHAPED TUNNELS

The tunnel at the experimental site near Gold Hill has an essentially flat floor and sides and a rounded top. (See Fig. 14.) For a plane wave incident on this tunnel, the calculated variation in field strength near the tunnel is not significantly different than that near a rectangular tunnel, but is different than the variation near a circular tunnel and a triangular tunnel. An example of this is illustrated in Fig. 15, which shows characteristic responses at 57 MHz for these tunnel shapes. It is seen that the flat surfaces (e.g., on square tunnels or the bottom of actual tunnels) seem to cause deeper minima than curved surfaces (e.g., on circular tunnels or the top of actual tunnels). The abrupt change in slope of the triangular tunnel has the deepest minima.

When we modeled tunnels with realistic shapes (as that in Fig. 14), we observed a phenomenon that was not as evident for right circular tunnels: the qualitative effect of the proximity of the source to the tunnel. As an example of the proximity effect, consider the difference

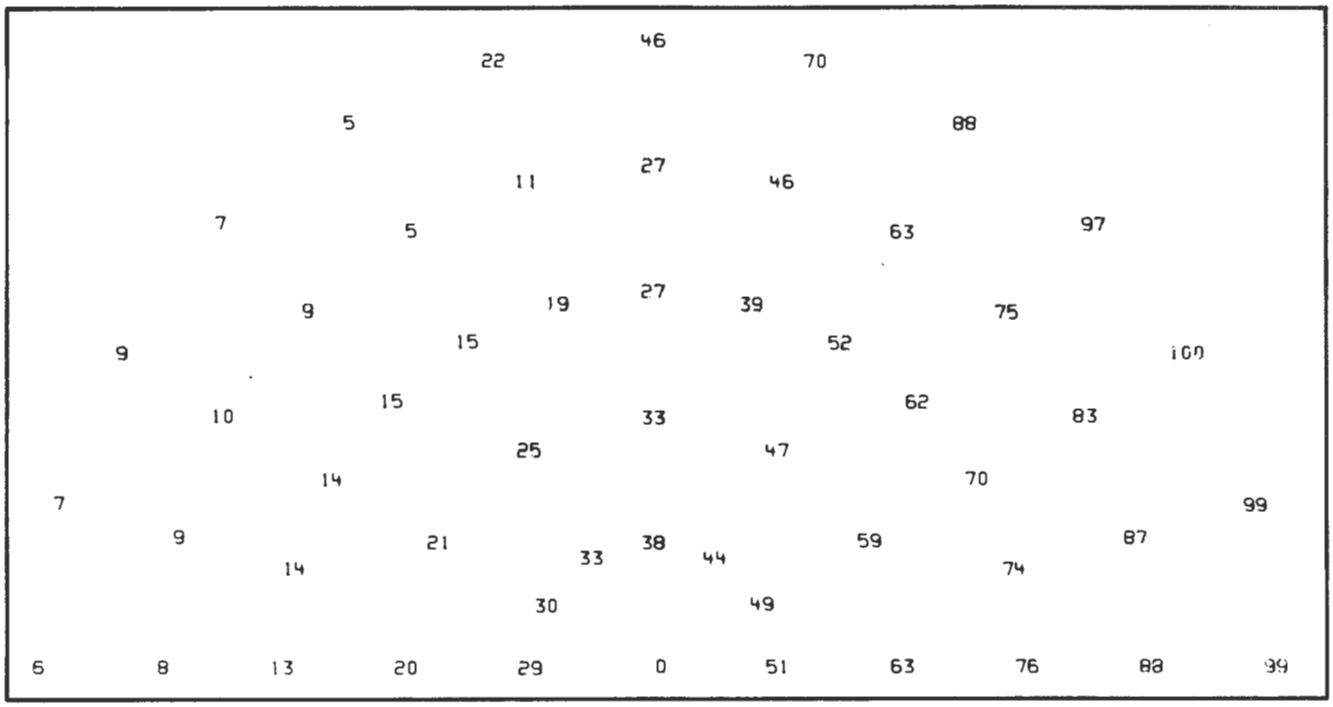

Fig. 12. Polarization currents, as shown by the relative magnitude of the electric field intensity resulting from plane-wave interaction.

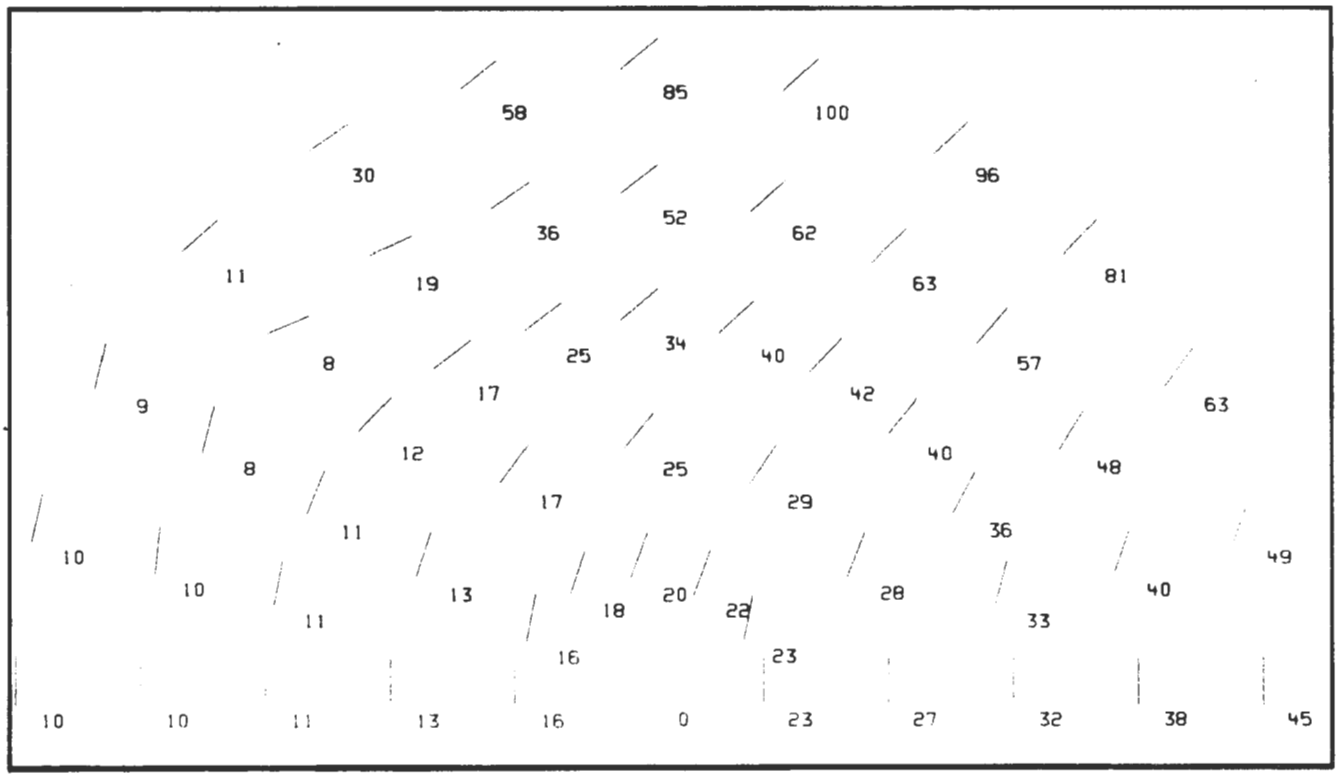

Fig. 13. Polarization of the induced field as shown by the magnetic field intensity inside the tunnel.

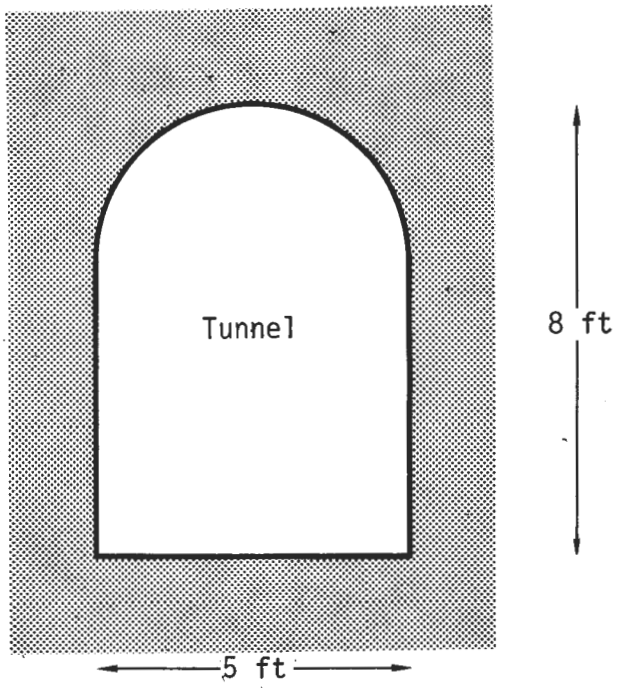

Fig. 14. The tunnel at the experimental site near Gold Hill, Colorado, has a cross section similar to this.

between responses due to a plane wave and those due to a line source. One can consider the plane wave to be due to a line source at infinity and at the same depth as the receiver. For both types of excitation, we present the calculated signal variation on the transmission side of a realistic tunnel at horizontal distances of 5, 35, and 64 feet from the tunnel edge. The plane-wave excitation results are shown in Fig. 16a, the line source excitation results in Fig. 16b. Note that the line-source excitation results maintain their deep minima to a greater distance from the tunnel than do the plane-wave excitation results. Thus, closer proximity of the source gives more pronounced interference, hence more noticeable signal minima. For a realistic tunnel shape and line source, when source and receiver are lowered in unison past the tunnel, the destructive interference (signal mimima) observed on the transmission side of the tunnel (see Fig. 17) is quite distinct and extends to a great distance.

An interesting question is, "What is the effect of the material inside the cavity or tunnel?" For all the results presented thus far, we have assumed that the tunnel was air filled. If the tunnel were filled with a material of the exact electrical character as the ambient medium, the tunnel would cause no variation in signal strength. This assumes that the tunnel causes no "halo" effect (discussed later). For a tunnel filled with a material of not quite the same electrical character as the ambient medium, the tunnel may still be observable, although its characteristic signature will be different from its signature when it is air filled. As shown in Fig. 18, the variation between maximum and minimum signal levels for the tunnel filled with a material of $\varepsilon_r = 12$ and $\sigma = 0$ is only 1.5:1, compared to the air filled tunnel max/min variation of 7:1. Thus, it

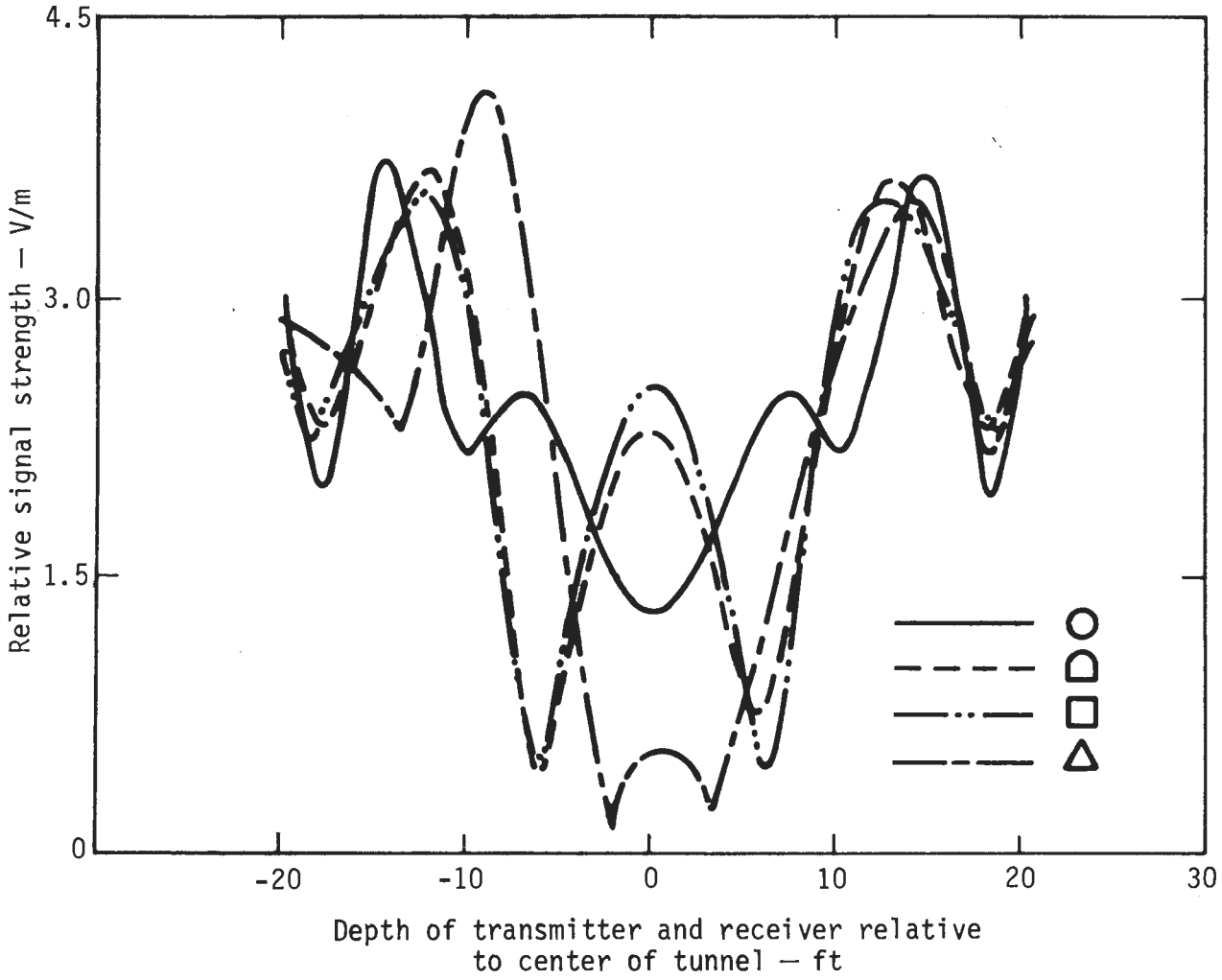

Fig. 15. Dependence on tunnel shape shown by theoretical signal variation for a frequency of 57 MHz with the transmitter 45 feet to one side of the tunnel and the receiver 35 feet to the other.

would be more difficult to detect the former tunnel, especially if there was significant geologic noise. One could even consider the variation from the backfilled tunnel to be similar to that of certain types of geologic noise.

Because the variation in signal strength depends on the actual shape of the tunnel, one might be suspicious of the ability to match theoretical with expreimental results. We have nevertheless attempted this, using the approximate theoretical solution for a line source interacting with the tunnel. The actual experimental situation would be better modeled by a point source rather than a line source, but this is expensive to compute. Also, the local medium

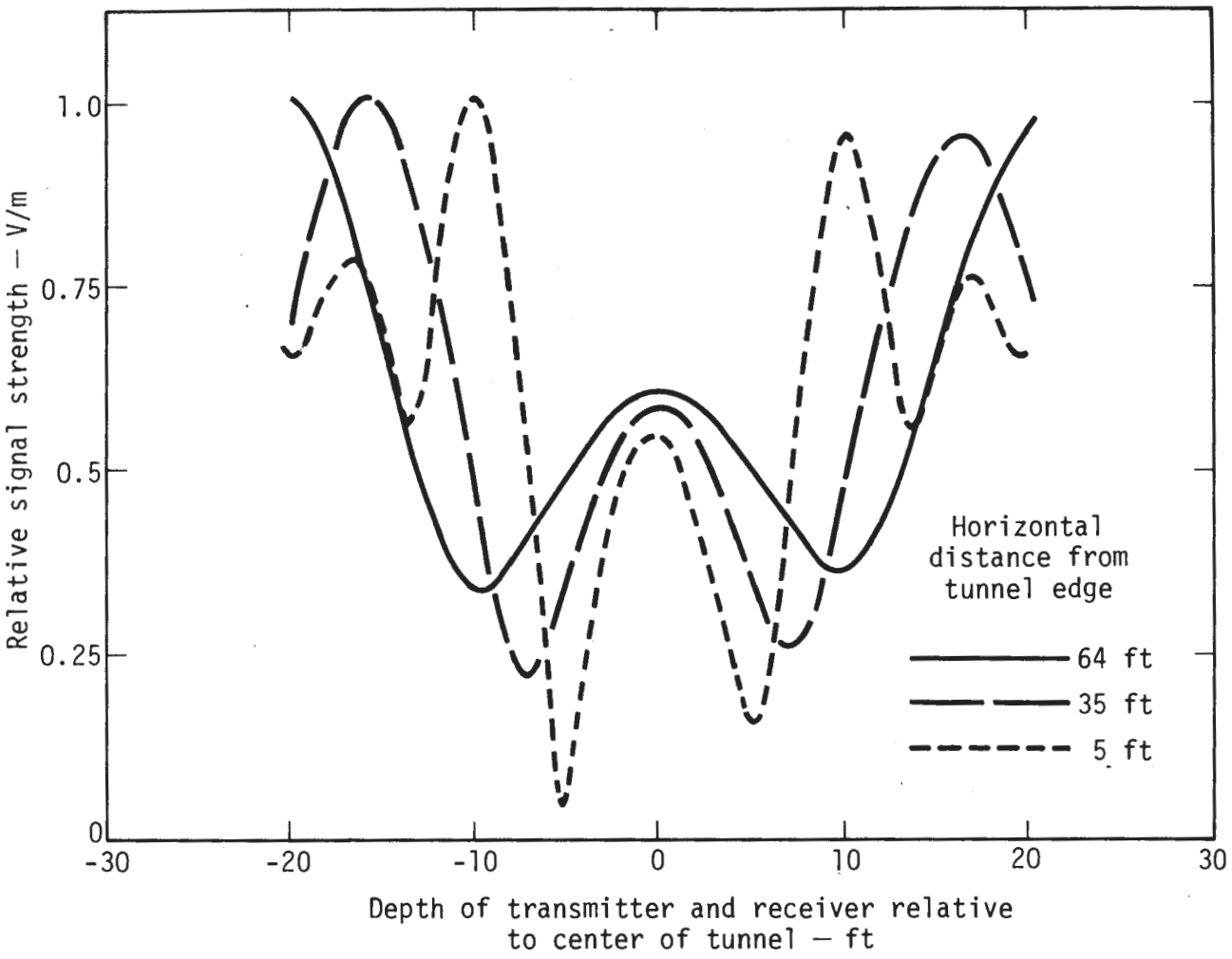

Fig. 16a. Signal minima are less deep at larger distances from the tunnel for a plane wave. Distances are on side away from transmitter.

was not homogeneous, so the experimentally recorded signal character includes geologic noise. Even with these qualifications, there still is a satisfactory fit between theory and experiment. (See Fig. 19.) This good agreement lends credence to our approach of data interpretation based on the theoretical modeling.

Another interesting question is, "What is the physical mechanism governing signal variation?" Due to the character of the modeled signal variation, we suspected that the dominant mechanism of interaction with the actual tunnel was diffraction, not reflection or refraction. As a test of this, we theoretically modeled the Fresnel diffraction of a perfectly conducting metallic strip and compared it with the calculated results for the Gold Hill tunnel.

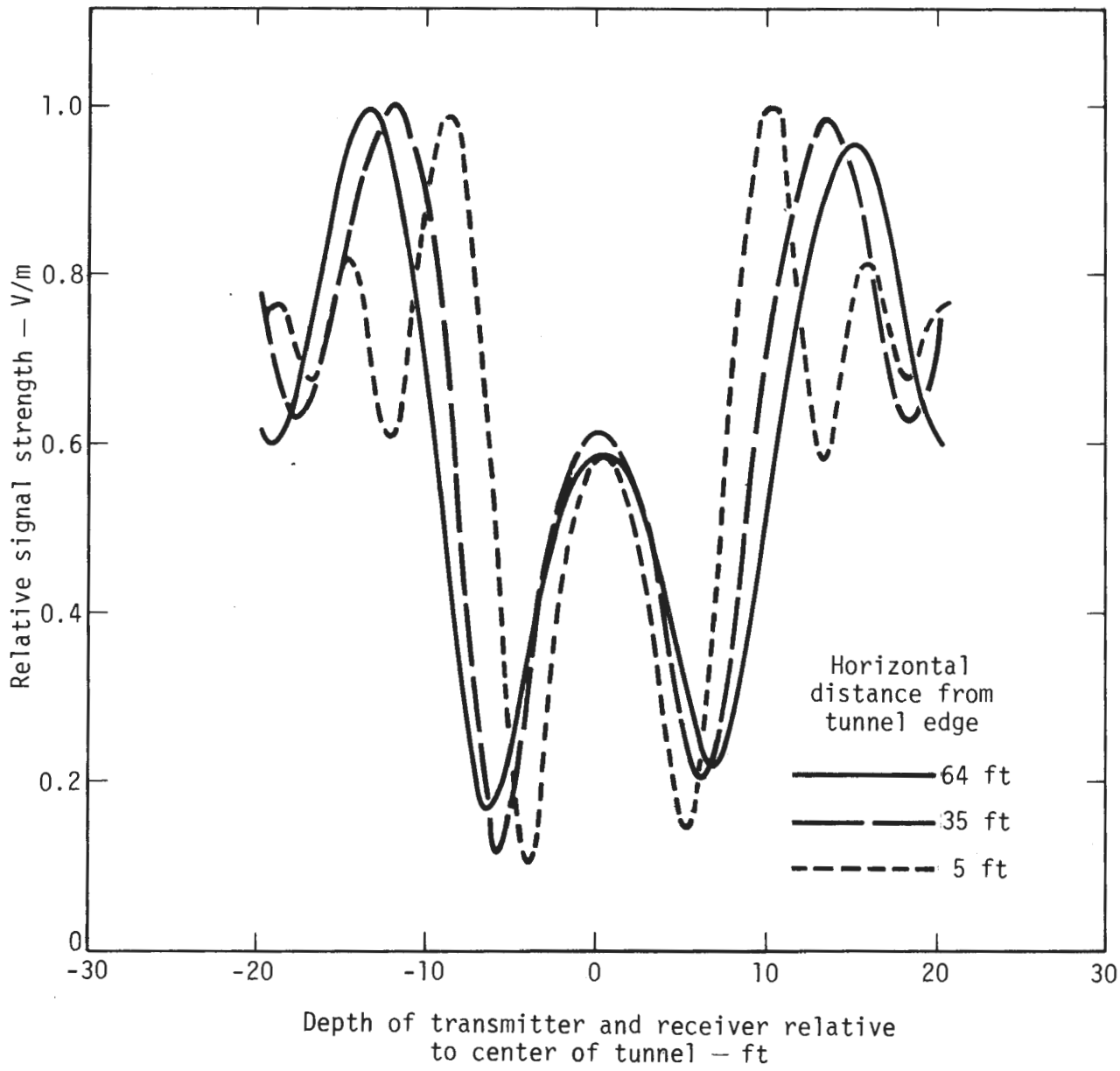

Fig. 16b. Signal minima from a line source are also less deep at larger distances from the tunnel. However, the signals from a line source maintain their minima to a much greater distance than those from a plane wave. Distances are on side away from transmitter.

(See Fig. 20.) This comparison showed the primary effect to be diffraction, especially in determining the locations of the signal minima (used for diagnosing the tunnel location). The high electrical contrast between tunnel and ambient media is primarily governed by displacement currents (due to relative dielectric contrast) rather than conduction currents (due to conductivity contrast) and may make the

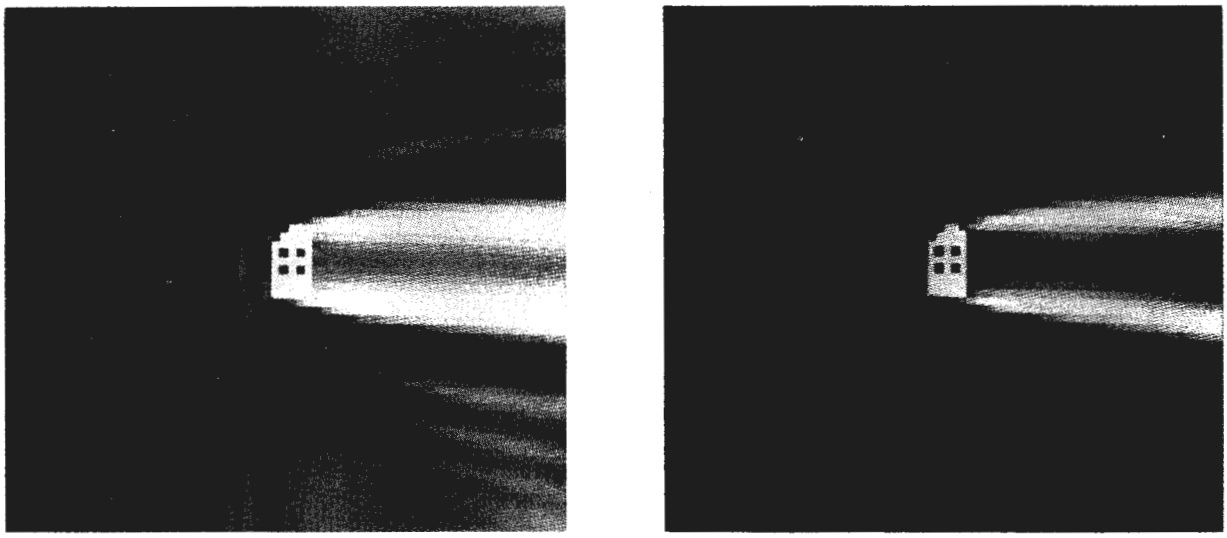

Fig. 17. The total field exterior to a tunnel of realistic shape. The frequency of excitation is 57 MHz. In (a) the transmitter is a line source of magnetic current parallel to the axis of the tunnel. The transmitter is located 45 feet to the left of the tunnel axis. Both source and receiver are lowered in unison past the tunnel. The horizontal axis extends 30 feet to either side of the tunnel, the vertical axis 30 feet above and below the tunnel.
(a) Line-source interaction.
(b) Plane-wave interaction.

tunnel interact similar to a perfectly conducting strip. This similarity deserves further investigation.

A number of individuals have asked, "What is the frequency dependence of this interaction?" or, more specifically, "What is a good frequency to use in detecting a tunnel or cavity with this method?" Theoretically, change of signal character with frequency for a realistic tunnel is not significantly different from the change with frequency for a right circular tunnel discussed earlier. We present in Fig. 21 the calculated variation of signal with depth for frequencies of 15, 30, 60, and 120 MHz. These results show the 60-MHz signal to theoretically be the easiest to diagnose. A signal of frequency 60 MHz, in a medium of $\varepsilon_r = 12$, has a λ_{medium} of about 1.4 m. The effective tunnel radius is about 4 ft or 1.25 m, which is about equal to this λ_{medium}. Thus, a wavelength of $\lambda_{medium} \approx b$ appears best for discerning a high contrast anomaly of radius b. This argument would hold for both electromagnetic and acoustic excitations.

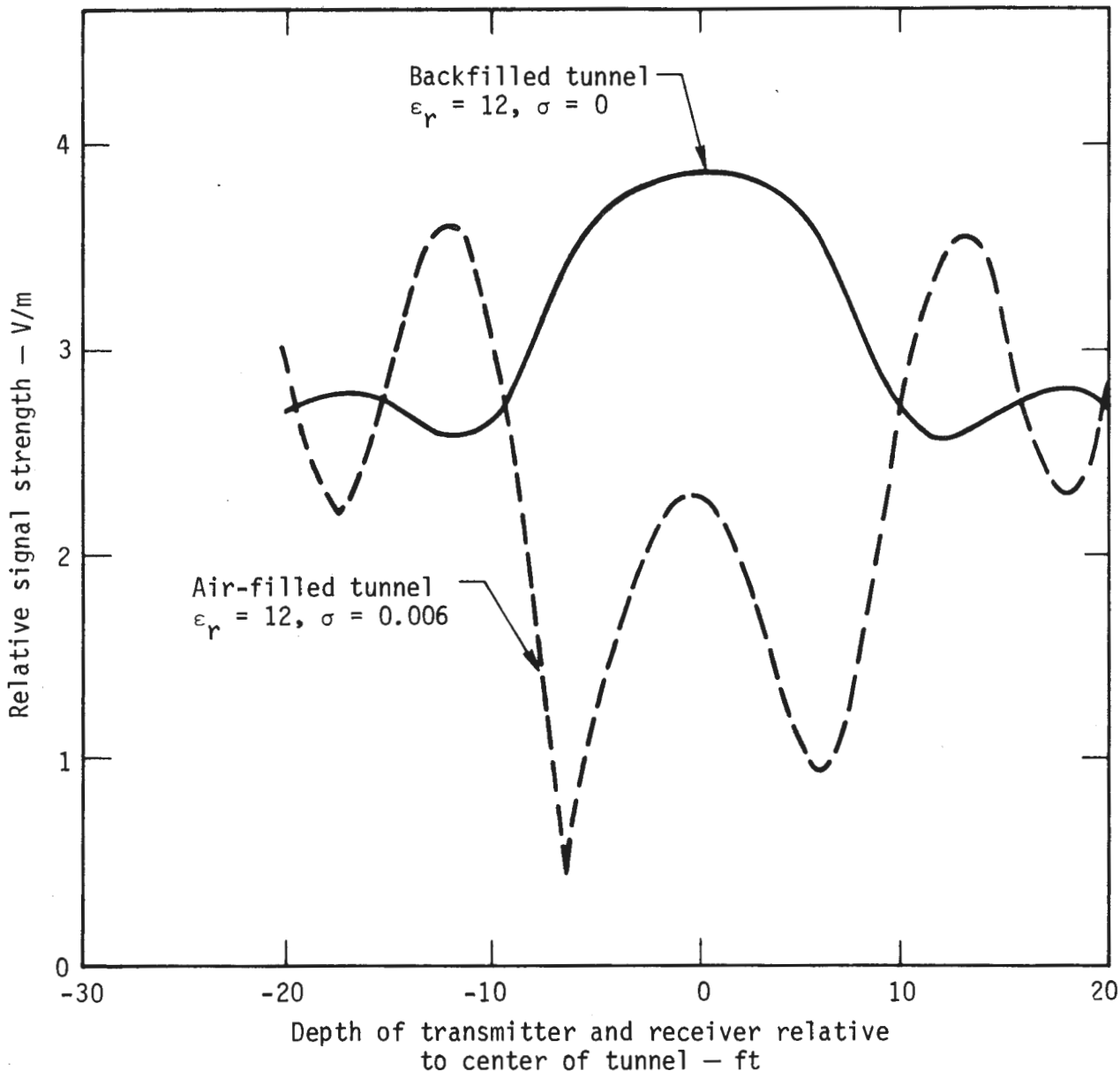

Fig. 18. Backfilled tunnel has much less signal variation than the air-filled tunnel.

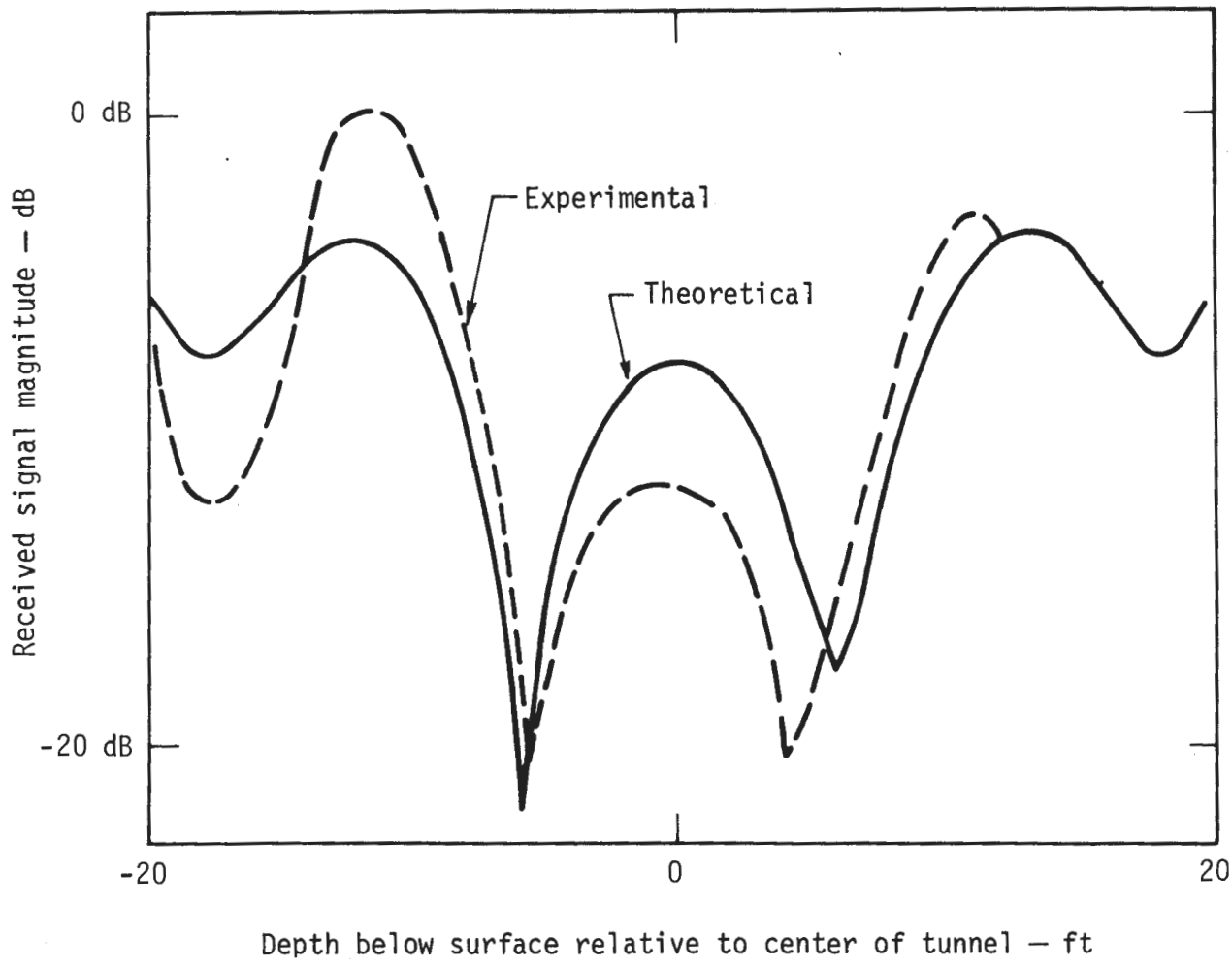

Fig. 19. Good agreement between theoretical and experimental variations for a realistically shaped tunnel. The frequency used was 57 MHz; receiver is in a drill hole 9 ft from the tunnel axis.

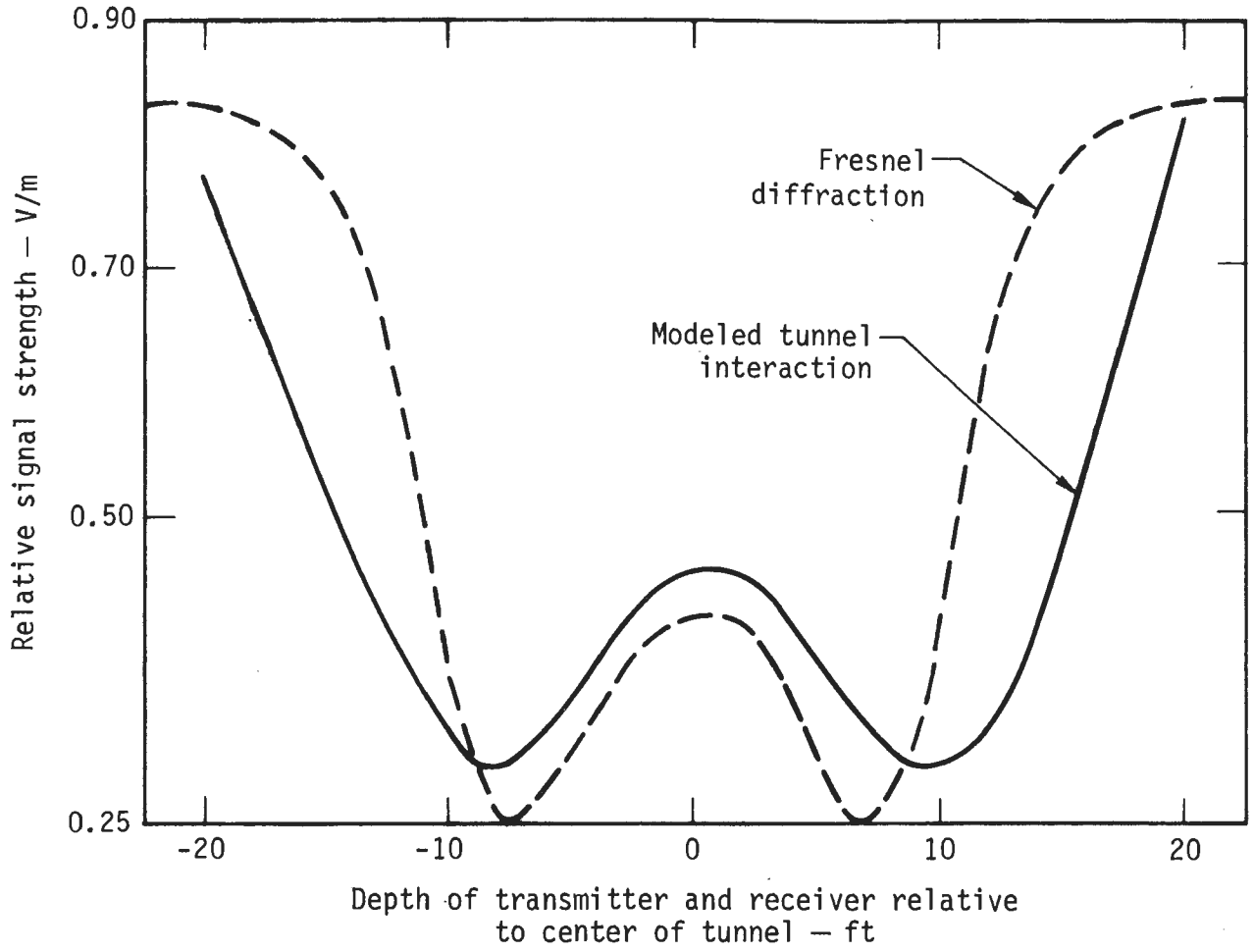

Fig. 20. Theoretical Fresnel diffraction is a good approximation of the modeled tunnel interaction.

For wavelengths of λ_{medium} much less than b/2, the small signal variation due to the tunnel would probably be lost in geologic noise. Signals with wavelengths much greater than b/2 would not propagate as far as signals with a wavelength of the order of b/2, and thus the preferable wavelength to use appears to be $\lambda_{medium} \cong b/2$.

From modeling the signal interaction with the right circular cylinder, we saw that the tunnel was not very detectable on the reflection side unless the receiver was quite close to the tunnel. As a spot check on this for a realistic tunnel shape, we computed the total signal at a position along a line approximately halfway between the source and the tunnel, shown in Fig. 22. Note that the absolute signal variation with depth is insignificant. For a continuous wave excitation the reflection mode is not as revealing as the transmission mode. The presence of the

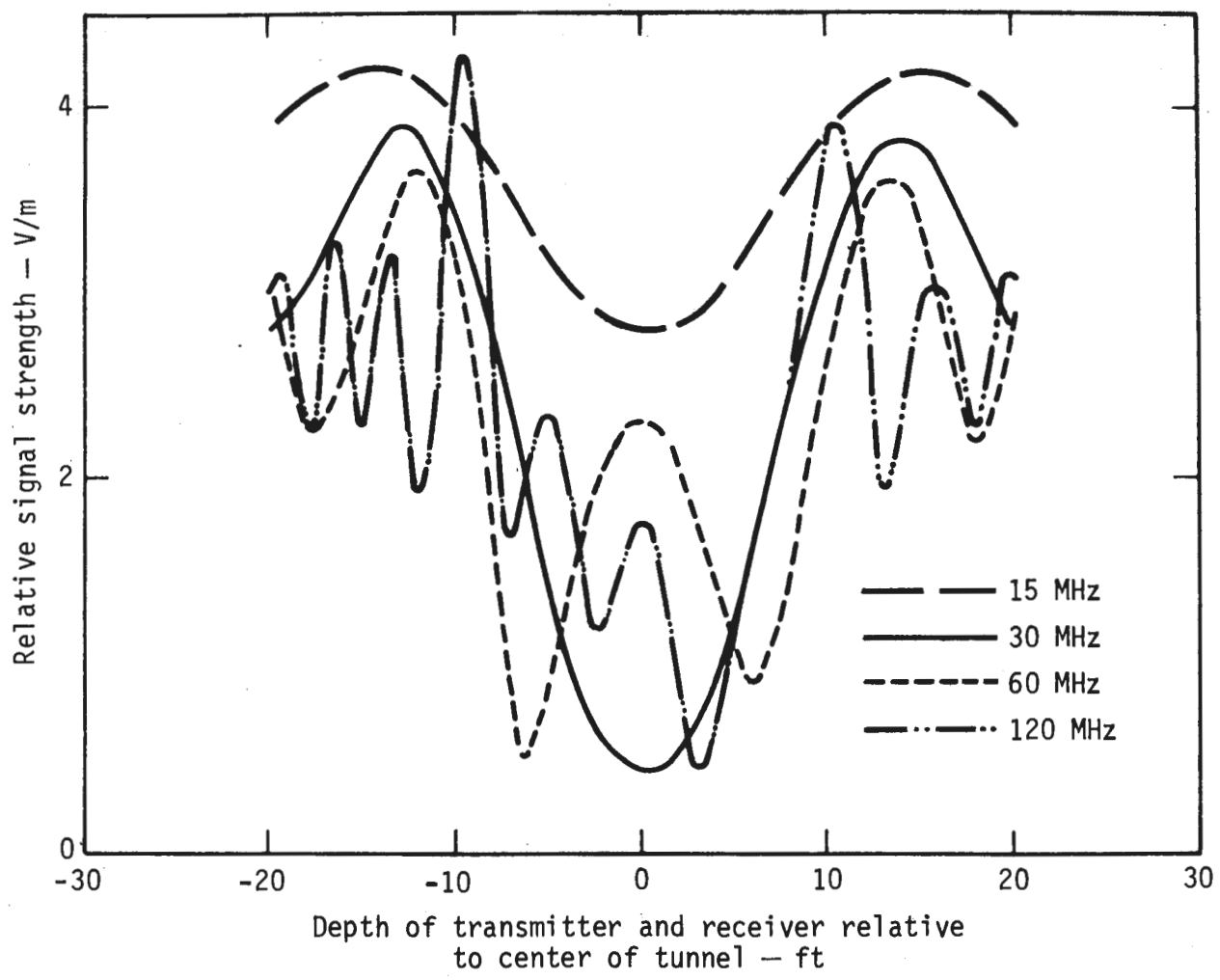

Fig. 21. Calculated response at various frequencies indicates a good diagnostic signal at 60 MHz. The modeled transmitter was 45 feet to one side of the tunnel, the receiver 35 feet to the other side.

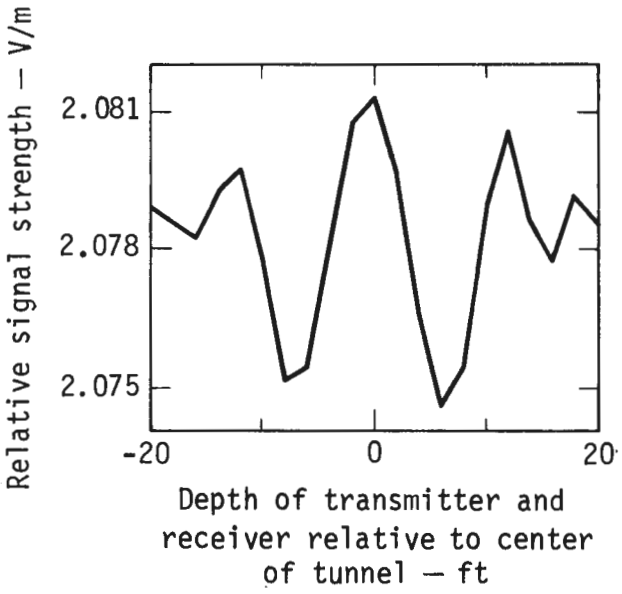

Fig. 22. The calculated signal about halfway between the transmitter and the tunnel shows little absolute variation with depth. The transmitter was 45 feet from the tunnel.

tunnel would be indiscernable from geologic noise for a signal variation similar to that shown in Fig. 22.

One other aspect we investigated was the effect of metallic rails on the tunnel floor on the transmission results. For a source 45 ft to one side of the tunnel and a receiver at 35 ft to the opposite side of the tunnel, metallic rails caused no measurable difference in the calculated signal for 57-MHz excitation. This was consistent with the experimentally observed minimal effect of a metallic screen placed in the tunnel, and with the postulated physical interaction governed by diffraction at the top and bottom of the tunnel.

Experimental Studies — Test Results from Gold Hill, Colorado

The Bureau of Mines agreed to let us use their test area near Gold Hill, Colorado. This test area has a tunnel passing through granite. We performed electromagnetic transmission experiments at this site to determine if electromagnetic propagation from drill hole to drill hole could be used to detect the presence of a tunnel and define its location.

When the experiments were performed (August 20-24, 1976), there were four usable drill holes near the tunnel. The depths of the drill holes and their locations relative to the tunnel axis are shown in Fig. 23. In the region of these drill holes, the tunnel is located between the depths of 76 ft and 84 ft. The width of the tunnel is 5 ft. We were able to accurately locate this tunnel using electromagnetic transmission, as explained below.

The transmission experiments are outlined in Figs. 24 and 25. Extensive measurements were made in the configuration of Fig. 24. Less data was taken for the configuration of Fig. 25 because of time and weather constraints. For the configuration of Fig. 24, data was taken for numerous transmitter and receiver depths at frequencies of 25, 57,

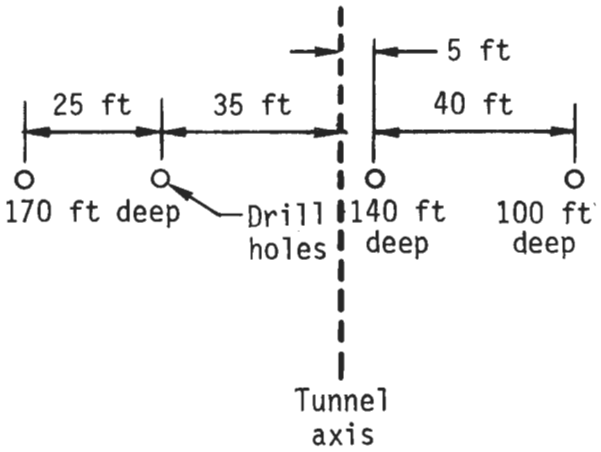

Fig. 23. Top view of the experimental site at Gold Hill, Colorado.

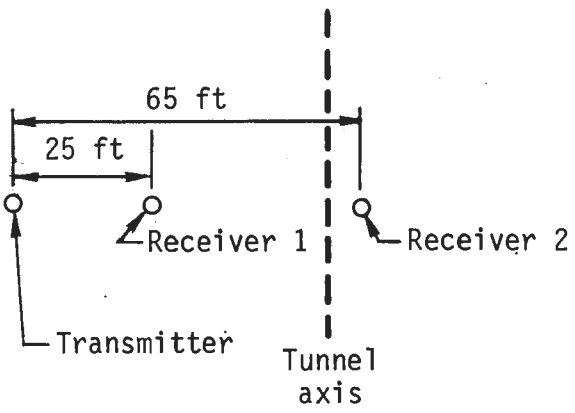

Fig. 24. Transmission over a total distance of 65 feet was achieved with this configuration.

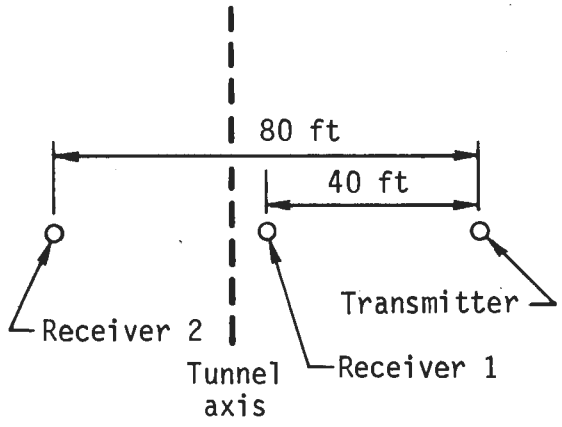

Fig. 25. Transmission over a total distance of 80 feet was achieved with this configuration.

and 80 MHz. Absolute signal levels in the two receiving holes were recorded, including both magnitude and phase of the received signals. However, our analysis of the experimental data has so far concentrated on the magnitude data. From the signal magnitudes in the two receiving drill holes, the difference in magnitudes between these two holes was also determined. A representative example of the recorded signal magnitude in two receiving holes and the associated difference in magnitude is depicted in Fig. 26. Note that we sampled the field at 2-ft intervals in the drill holes. The rapid variation in signal strength suggests that a continuous recording versus depth is desired.

It is noted from Fig. 26 that the signal on the transmission side of the tunnel (80 ft from transmitter) has more variation (and perhaps more useful information) than the signal on the reflection side of the tunnel (40 ft from the transmitter). This observation is consistent with the previously presented theoretical prediction that the reflection side would not have a significant signal variation.

To further acquaint the reader with the site character, we note that the measured relative dielectric constant ε_r was approximately 12 for all the frequencies used, and the conductivity σ was 0.003 S/m at 25 MHz, 0.005 S/m at 57 MHz, and 0.007 S/m at 80 MHz. In the theoretical models presented previously, we assumed that the ambient medium was homogenous with $\varepsilon_r = 12$ and $\sigma = 0.006$ S/m for all frequencies. The tunnel was modeled as

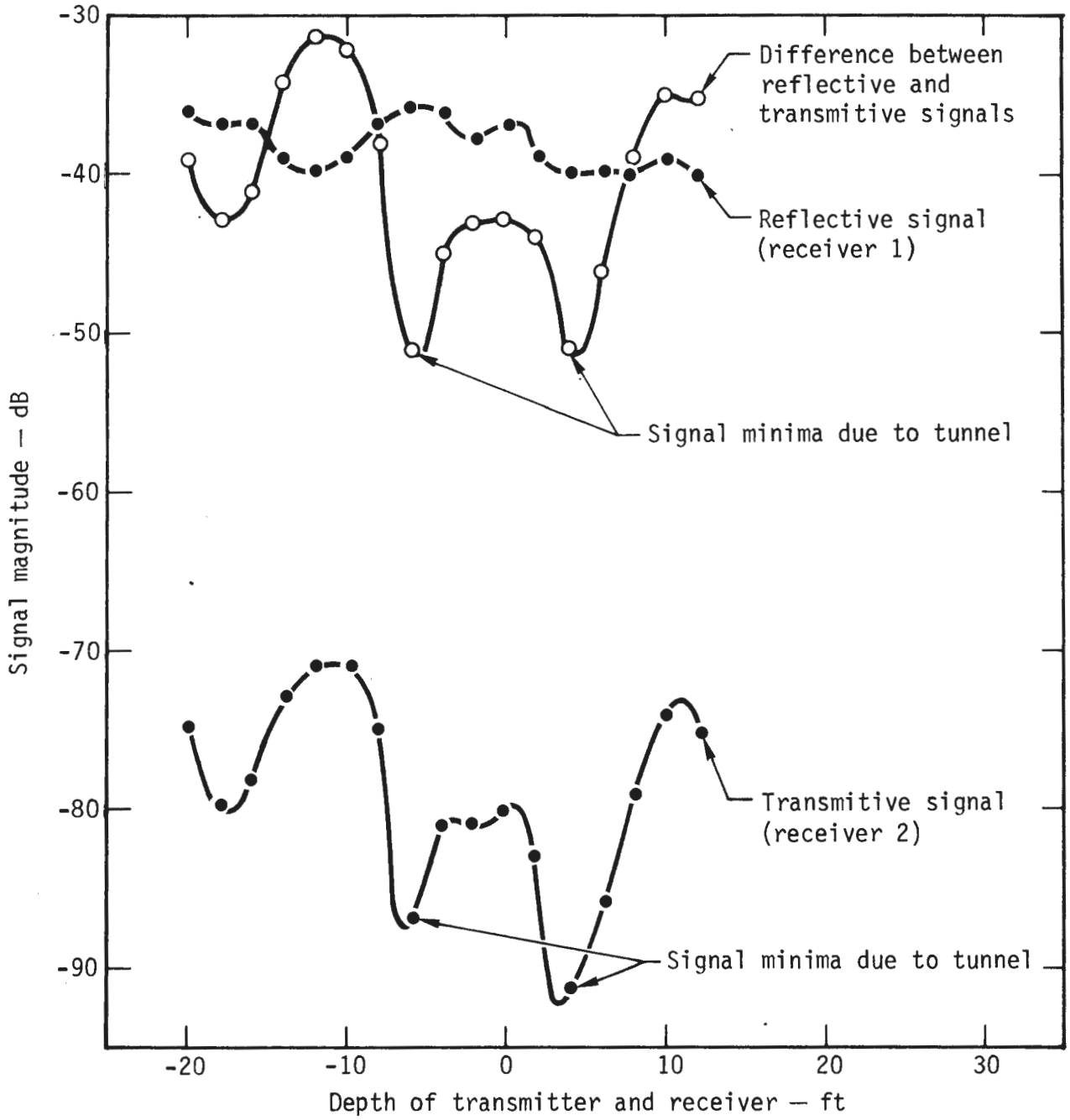

Fig. 26. Representative data set for the configuration given in Fig. 25.

having the electrical parameters $\varepsilon_r = 1$ and $\sigma = 0$.

While performing the experiments at the Gold Hill site, it became apparent that the electromagnetic interaction with the tunnel was governed by diffraction, not straight line ray optics. That is, sharp variations in signal strength were observed within vertical distances of 4 ft or less. (See Fig. 26.). The quasi-periodic nature of the variations are not characteristic of ray optics (even including refraction) but could be from diffraction. Repeated transmission measurements with a metal screen along the tunnel wall also indicated diffraction was the dominant mechanism. This screen caused very little difference in the transmission results. We have also noted this apparent diffraction effect in scale modeling experiments (100:1 size reduction), using a water tank and a Bakelight anomaly to model a large contrast between the propagation constants in the ambient medium and an electrical anomaly.

It was apparent that a data-interpretation method based on ray optics would not adequately describe the phenomena observed at Gold Hill. The ray optical approach has been adequate when the medium parameters vary sufficiently slowly from point to point. However, for finding tunnels, the rapid change in the electrical propagation constant at the tunnel/granite boundary requires a modeling and data-interpretation scheme including the effects of diffraction.

Interpretation of the Experimental Data

By using the back projection technique discussed earlier on the data obtained at Gold Hill, we estimated the location of the tunnel. For the configuration of Fig. 24 (65-ft maximum separation), detailed data were taken for six views. A display of the six views taken at a frequency of 57 MHz is given in Fig. 27. Remember that each view yields an interpretation that the tunnel lies within a sector defined by the two lowest minima in the transmission results. The region where all of the views coincide should contain the tunnel.

Because of the large amount of data taken for the particular situation of Fig. 27, the tunnel region is reasonably well defined. The estimated most probable horizontal location of the tunnel is quite accurate (within 2 ft). The estimated most probable depth of the

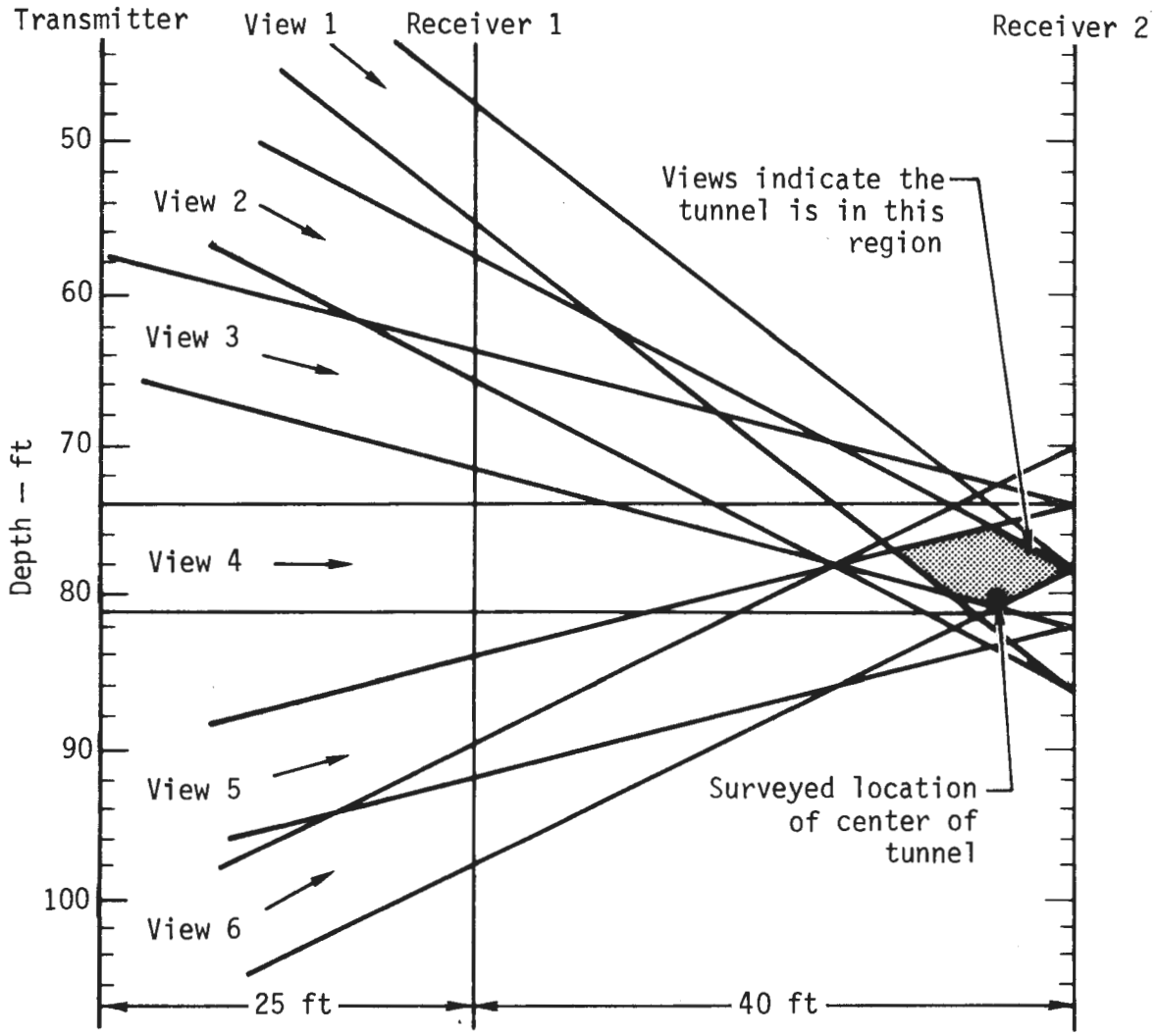

Fig. 27. Superposition of the six views indicates the most probable tunnel location to within three feet of the surveyed tunnel location. Transmitter/receiver configuration is that of Fig. 24; frequency used was 57 MHz.

tunnel is also reasonably accurate (within 5 ft). The deep minima indicating the presence of the tunnel and the internal consistency of our collected data supporting this indication are quite strong.

The configuration of Fig. 24 was also used to record some data at frequencies of 25 MHz and 80 MHz. These data were recorded only for a horizontal view. The data at 25 MHz showed a small variation of 3 dB over the background level in the vicinity of the tunnel and would not permit a confident prediction of the tunnel location. This is similar to the effect predicted theoretically. The data at 80 MHz were similar in quality to those at 57 MHz, except the signal variation with

depth was even more rapid. This is also in agreement with theoretical predictions. After noting this, we thereafter recorded the data at 57 MHz, as this gave a significant signal variation in the vicinity of the tunnel, and would propagate farther than an 80-MHz signal. The lower frequency also would not be as severely influenced by small localized inhomogeneities in the medium.

A limited amount of data was taken for the configuration of Fig. 25 (80-ft maximum separation) at a frequency of 57 MHz. Even with this limited data, the estimated most probable depth of the tunnel was quite accurate (within 2 ft; see Fig. 28). There really are not enough views to be able to confidently predict the horizontal location of the tunnel. However, it is interesting to note that the center of the region where all the views are superimposed is horizontally within 7 ft of the center of the tunnel.

Conclusions

- The presence of and the horizontal and vertical positions of a tunnel or cavity can be determined by cross-borehole, continuous-wave electromagnetic or acoustic transmission. This has been demonstrated both theoretically and experimentally for electromagnetic transmission and theoretically for acoustic transmission.

- The simple data interpretation algorithm used in this report enables the experimenter to quickly and easily interpret the data in the field. No computations are required for interpretation; one needs only the records of signal magnitude, a ruler, a pen, and graph paper.

- For a tunnel or cavity radius b, the data signature is easy to interpret if $\lambda_{medium} \cong b/2$. This applies for both electromagnetic and acoustic continuous wave excitations.

- The signal on the transmission side of the tunnel or cavity typically has more variation (and is thus easier to interpret in the presence of geologic noise) than that on the reflection side of the tunnel or cavity.

- The physical mechanism governing signal transmission appears to be similar to Fresnel diffraction from a perfectly conducting metallic strip. One possible explanation for this is the high electrical contrast of the tunnel with the ambient medium, which makes the perfect tunnel behave similar to a perfectly conducting metallic strip.

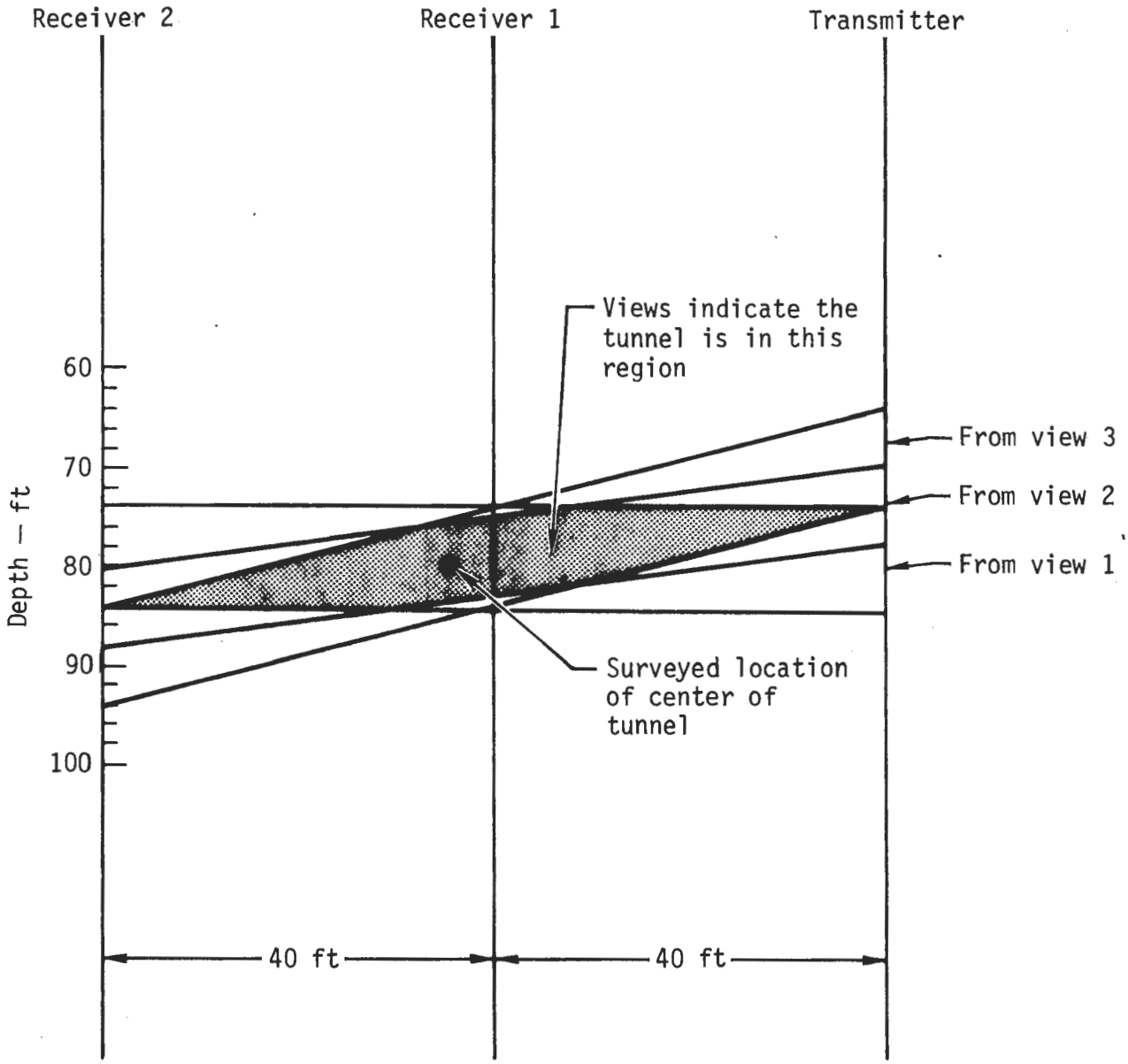

Fig. 28. Superposition of the three views indicates the most probable tunnel location to within seven feet of the surveyed tunnel location. Transmitter/receiver configuration is that of Fig. 25; frequency used was 57 MHz.

- The presence of other high electrical contrast anomalies (such as rails) within a tunnel does not significantly alter these conclusions in the situations studied. However, the presence of material within a tunnel with electrical parameters similar to the ambient medium significantly reduces the detectability of the tunnel.

Recommendations

Because of the rapid variation of the signal with distance, the signal in a drill hole should be sampled at least every foot. Continuous recording of signal variation with depth would be even better. This would require modifying our cable reels for transmitter and receiver. As the data are easily reduced in the field if the spatial separation and orientation are kept fixed (i.e., the data are recorded for a particular view), the equipment should also be modified so that the transmitter and receiver cables can be continuously lowered and raised in unison. Neither the continuous spatial record nor the linking of transmitter and receiver raising and lowering is an especially difficult task. These modifications should be incorporated into the system.

Although we have been able to use a simple data-interpretation algorithm, it has only been used to reduce data obtained at a relatively clean geologic site. The basic idea of discerning the presence of and locating a high contrast anomaly will undoubtedly be given practical application at a more geologically complex site. We have not yet studied the effect of an inhomogeneous medium on the characteristic signal variations. The effects of small and large scale inhomogeneities should be studied, especially with regard to successful interpretation of data to locate any high contrast anomalies. The masking of one anomaly by another may be one problem in such a medium. By using the complete data records for each of the views, rather than just the minima of the various views, it may be possible to invert the data and obtain an accurate electromagnetic profile for the complete region between the drill holes, rather than obtaining just the location of the tunnel. Attempts to improve the overall resolution in this way should be made. Our first attempt at improving resolution was to use back projection in the classical sense.[3]

The data interpretation results in this report are encouraging, but also indicate that further sophistication or other approaches are needed to obtain good resolution of the complete region between the drill holes (when the region contains a high contrast anomaly). Techniques exist for good resolution of a region containing a low-contrast anomaly.[1] A number of alternative interpretation algorithms should be developed in an effort to achieve this objective.

It has been noted[2,18] that, in many instances, the apparent scattering cross-section of anomalies

in the earth is much larger than one might expect (a halo effect). This has been attributed to possible differences in the water profile caused by the anomaly, to fractures reaching beyond the apparent anomaly size, or to increased weathering effects about the anomaly due to a combination of the above. Thus, attention in modeling and experiments should be directed not only to the obvious anomaly (e.g., an absence of rock for a tunnel), but to the overall electrical anomaly.

Acknowledgments

Financial support for the theoretical and interpretational aspects of this work was granted by Mr. R. K. MacFarland of the Department of Transportation. Support for the experimental aspects was supplied by Dr. E. Blase of the Advanced Research Projects Agency. Also noteworthy are helpful discussions held with Mr. R. Myers of the Bureau of Mines, Dr. B. James of the Advanced Research Projects Agency, and Dr. E. Miller of the Lawrence Livermore Laboratory.

FW/gw/vt/gw

References

1. D. L. Lager and R. J. Lytle, *Radio Science,* in publication.

2. E. F. Laine, "Using Resistivity Measurements to Detect Caverns in Coal Mines," Lawrence Livermore Laboratory Rept. UCRL-77507, November 1975.

3. G. T. Herman and S. A. Johnson, *Scientific American 233* (4), 56 (1975).

4. H. Zaklad, *Electronics 49* (21), 89 (1976).

5. R. J. Lytle, E. F. Laine, and D. L. Lager, "Using Electromagnetic Remote Probing to Determine the Physical Properties of a Coal Seam," presented at the Society of Exploration Geophysicists Annual Meeting, Denver, Colorado, October 1975; also presented at the American Nuclear Society Annual Meeting, San Francisco, California, November 1975.

6. P. Bois, M. LaPorte, M. Lavergne, G. Thomas, *Geophysics 37*, 471 (1972).

7. M. Kaspar and J. Pecen, *Geophysical Prospecting 23*, 611 (1975).

8. J. R. Wait, *Can. J. Phys. 33*, 189 (1955).

9. G. Tyras, *Radiation and Propagation of Electromagnetic Waves,* (Academic Press, New York, 1969), pp. 274-280.

10. D. E. Barrick, Chapter 4 of *Radar Cross Section Handbook, Volume 1,* H. T. Ruck, Ed. (Plenum Press, New York, 1970), pp. 205-339.

11. R. J. Lytle, *IEEE Trans. on Antennas and Propagation AP-19* (5), 618 (1971).

12. R. J. Lytle and D. L. Lager, *Radio Science 11* (4), 245 (1976).

13. J. H. Richmond, *IEEE Trans. on Antennas and Propogation AP-14*, 460 (1966).

14. G. W. Hohmann, *Geophysics 36*, 101 (1971).

15. J. R. Parry and S. H. Ward, *Geophysics 36*, 67 (1971).

16. J. H. Coggon, *Geophysics 36*, 132 (1971).

17. T. B. A. Senior and P. L. E. Uslenghi, "Chapter 2, The Circular Cylinder," in *Electromagnetic and Acoustic Scattering by Simple Shapes,* J. J. Bowman, T. B. A. Senior, P. L. E. Uslenghi, Eds. (North-Holland Publishing Company, Amsterdam, Netherlands, 1969), pp. 92-128.

18. J. Lapajne, "Some Remarks About the Geoelectrical Exploration of Buried Bodies," paper presented at the European Association of Exploration Geophysicists Silver Anniversary Meeting, The Hague, Holland, June 1976.

Appendix A
Exact Equations Describing Fields Due to a Line Source Interacting with a Right Circular Tunnel

For an electric line source of current I_e located at position $\vec{\rho}_s$ [or (ρ_s, ϕ_s)] external to a cylinder of radius a (see Fig. A-1), the received field E_z at position $\vec{\rho}_r$ [or (ρ_r, ϕ_r)] is:

$$E_z = -\frac{k_{out}^2 I_e}{4\omega\varepsilon_{out}} \left[H_0^{(2)}(k_{out}|\vec{\rho}_s - \vec{\rho}_r|) \right.$$

$$- \sum_{m=0}^{\infty} (2-\delta_{0m}) \cos m(\phi_r - \phi_s) H_m^{(2)}(k_{out}\rho_s) H_m^{(2)}(k_{out}\rho_r) \cdot$$

$$\left. \cdot \frac{J_m(k_{out}a) - Z_e J_m'(k_{out}a)}{H_m^{(2)}(k_{out}a) - Z_e H_m^{(2)'}(k_{out}a)} \right]$$

for $\rho_r \leq \rho_s$. The fields H_ρ and H_ϕ can be obtained by:

$$H_\rho = -\frac{1}{j\omega\mu_0\rho} \frac{\partial E_z}{\partial \phi},$$

$$H_\phi = \frac{1}{j\omega\mu_0} \frac{\partial E_z}{\partial \rho}.$$

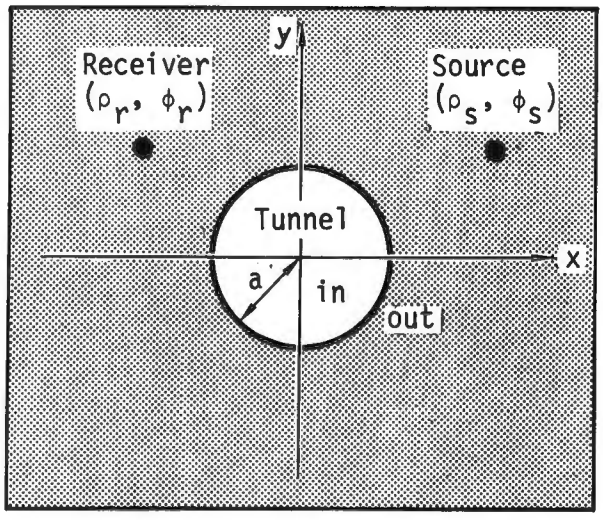

Fig. A-1. Model used for exact calculation of the fields excited by a line source of current around a right circular tunnel.

For an electric line-current excitation, the field components E_ρ, E_ϕ, and H_z are zero.

In the above expressions, $\delta_{0m} = 1$ if $m = 0$,

$$\delta_{0m} = 0 \text{ if } m \geq 1,$$

$$Z_e = \frac{\mu_0 J_m(k_{in}a)}{J'_m(k_{in}a)} \cdot \frac{k_{out}}{k_{in}} ,$$

$$k_{out}^2 = \omega^2 \mu_0 \varepsilon_{out} ,$$

$$k_{in}^2 = \omega^2 \mu_0 \varepsilon_{in} ,$$

$$\varepsilon_{out} = \varepsilon_0 \varepsilon_{r_{out}} - j\sigma_{out}/\omega ,$$

$$\varepsilon_{in} = \varepsilon_0 \varepsilon_{r_{in}} - j\sigma_{in}/\omega .$$

For a magnetic line source of current I_m located a position $\vec{\rho}_s$ external to a cylinder of radius a, the received field H_z at position $\vec{\rho}_r$ is:

$$H_z = -\frac{k_{out}^2 I_m}{4\omega\mu_0} \left[H_0^{(2)}(k_{out}|\vec{\rho}_s - \vec{\rho}_r|) \right.$$

$$- \sum_{m=0}^{\infty} (2-\delta_{om}) \cos m(\phi_t - \phi_r) H_m^{(2)}(k_{out}\rho_s) H_m^{(2)}(k_{out}\rho_r)$$

$$\left. \cdot \frac{J'_m(k_{out}a) - Z_m J_m(k_{out}a)}{H_0^{(2)'}(k_{out}a) - Z_m H_m(k_{out}a)} \right],$$

for $\rho_r \leq \rho_s$. In this expression,

$$Z_m = \frac{\mu_0 J'_m(k_{in}a)}{J_m(k_{in}a)} \cdot \frac{k_{out}}{k_{in}} .$$

The fields E_ρ and E_ϕ can be obtained by:

$$E_\rho = \frac{1}{j\omega\varepsilon_{out}\rho} \frac{\partial H_z}{\partial \phi} ,$$

$$E_\phi = - \frac{1}{j\omega\varepsilon_{out}} \frac{\partial H_z}{\partial \rho} .$$

For a magnetic line current excitation, the field components H_ρ, H_ϕ, and E_z are zero.

The fields external to the cylinder (in the region $a \leq \rho_s \leq \rho_r$) and internal to the cylinder (in the region $\rho_r \leq a \leq \rho_s$) may be similarly expressed. The details of these formulas are omitted for brevity.

When the source is removed to an electrically large distance from the cylinder, the asymptotic behavior of the large argument Hankel function can be used:

$$H_m^{(2)}(k\rho) \xrightarrow[|k\rho|\to\infty]{} \sqrt{\frac{2}{\pi k\rho}} \exp(-jk\rho + j\pi/4 + jm\pi/2).$$

In addition, when $|k_{out} (\vec{\rho}_s - \vec{\rho}_r)| >> 1$, then

$$H_0^{(2)}(k_{out}|\vec{\rho}_s - \vec{\rho}_r|) \cong \sqrt{\frac{2j}{\pi k_{out}\rho_s}} \exp(-jk_{out}|\vec{\rho}_s - \vec{\rho}_r|)$$

for $\rho_r << \rho_s$. By the law of cosines, one can show for this situation that

$$|\vec{\rho}_s - \vec{\rho}_r| \cong \rho_s - x_r \cos\phi_s - z_r \sin\phi_s,$$

and thus,

$$H_0^{(2)}(k_{out}|\vec{\rho}_s - \vec{\rho}_r|) \cong \sqrt{\frac{2j}{\pi k_{out}\rho_s}} \exp(-jk_{out}\rho_s)$$

$$\cdot \exp(+ jk_{out}x_r \cos\phi_s + jk_{out}z_r \sin\phi_s).$$

By using these results, one can show that when $|k_{out}\rho_s| >> 1$ and $\rho_s >> \rho_r$, then the field E_z due to an electric line current I_e is:

$$E_z = -\frac{k_{out}^2 I_e}{4\omega\varepsilon_{out}}\sqrt{\frac{2}{\pi k_{out}\rho_s}}\ \exp(-jk_{out}\rho_s + j\pi/4)$$
$$\cdot\left[\exp(+jk_{out}\rho_r)\right.$$
$$\left. - \sum_{m=0}^{\infty} (2-\delta_{0m})\cos m(\phi_s-\phi_r)\ H_m^{(2)}(k_{out}\rho_r)\ j^m\ \frac{J_m(k_{out}a)-Z_e J_m'(k_{out}a)}{H_m^{(2)}(k_{out}a)-Z_e H_m^{(2)'}(k_{out}a)}\right].$$

and the field H_z due to a magnetic line current I_m is:

$$H_z = -\frac{k_{out}^2 I_m}{4\omega\mu_0}\sqrt{\frac{2}{\pi k_{out}\rho_s}}\ \exp(-jk_{out}\rho_s + j\pi/4)$$
$$\cdot\left[\exp(+jk_{out}\rho_r)\right.$$
$$\left. - \sum_{m=0}^{\infty} (2-\delta_{0m})\ \cos m(\phi_s-\phi_r)\ H_m^{(2)}(k_{out}\rho_r)\ j^m\ \frac{J_m'(k_{out}a)-Z_m J_m(k_{out}a)}{H_m^{(2)'}(k_{out}a)-Z_m H_m^{(2)}(k_{out}a)}\right].$$

Appendix B
The Approximate Equations Describing Fields Due to a Line Source Interacting with a Tunnel of Arbitrary Cross-Section

Approximate solutions for scattering of electromagnetic waves by cylinders of arbitrary cross section can be obtained with the aid of a digital computer. Consider, as in Fig. B-1, an infinitely long cylinder with axis parallel to the z axis. We restrict our attention to the case of an incident harmonic wave with electric field normal to the axis of the cylinder (TE mode). Thus, after suppressing the time variation factor $\exp(j\omega t)$, where $\omega = 2\pi f$ is the radian frequency and f is the frequency in Hertz of the electromagnetic waves, we obtain for the incident field:

$$\underline{E}^i = \hat{x}\, E^i_x(x,y) + \hat{y}\, E^i_y(x,y). \tag{B-1}$$

First, one divides the cross section into rectangular cells small compared to the wavelength of the field so that the field within a cell is approximately uniform. The fields at the individual cells can then be related to the incident field by the following two equations:

$$\sum_{n=1}^{N} (A_{mn} E_{xn} + B_{mn} E_{yn}) = E^i_{xm}, \tag{B-2}$$

$$\sum_{n=1}^{N} (C_{mn} E_{xn} + D_{mn} E_{yn}) = E^i_{ym}, \tag{B-3}$$

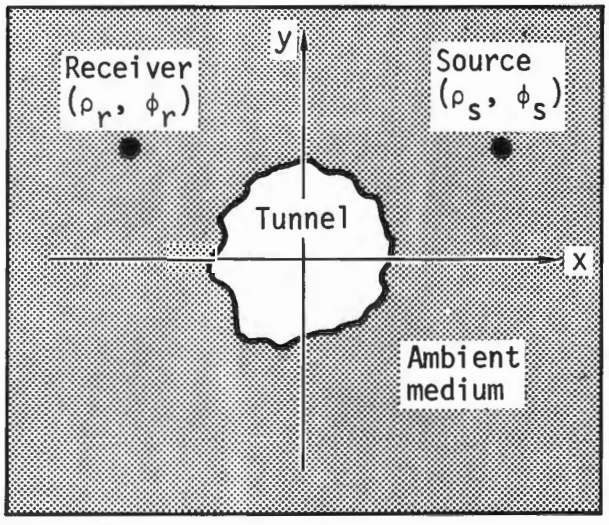

Fig. B-1. Model used for approximate calculation of the fields excited by a line source of current around a tunnel of arbitrary shape.

where N is the number of cells in the cross section, E^i_{xm} and E^i_{ym} are the $\vec{x}$ and $\vec{y}$ components, respectively, of the incident field in the m^{th} cell, and E_{xn} and E_{yn} are the $\vec{x}$ and $\vec{y}$ components, respectively, of the field in the n^{th} cell. There are 2N such equations, the coefficients of which are given by:

$$A_{mn} = K'\left[k\rho(y_m - y_n)^2 H_0(k\rho) + [(x_m - x_n)^2 - (y_m - y_n)^2]H_1(k\rho)\right], \tag{B-4}$$

$$B_{mn} = C_{mn} = K'(x_m - x_n)(y_m - y_n)[2H_1(k\rho) - kH_0(k\rho)], \tag{B-5}$$

$$D_{mn} = K'\left[k\rho(x_m - x_n)^2 H_0(k\rho) + [(y_m - y_n)^2 - (x_m - x_n)^2]H_1(k\rho)\right], \tag{B-6}$$

for $m \neq n$, and

$$A_{mm} = D_{mm} = 1 + (\varepsilon_m - 1)[0.25j\pi k a_m H_1(ka_m) + 1], \tag{B-7}$$

$$B_{mm} = C_{mm} = 0, \tag{B-8}$$

for the diagonal elements (m = n). In Eqs. (B-4) through (B-8):

$$K' = j\pi a_n J_1(ka_n)(\varepsilon_n - 1), \tag{B-9}$$

and

$$\rho = \sqrt{(x_m - x_n)^2 + (y_m - y_n)^2}\,, \tag{B-10}$$

where a_n is the radius of a circle with the same area as the n^{th} rectangular cell; $k = 2\pi/\lambda$, where λ is the wavelength in the ambient medium; $J_1(ka_n)$ is the Bessel function of order one; ε_n is the dielectric constant of the n^{th} cell relative to the ambient medium; ρ is the distance between the n^{th} and m^{th} cells; x_n and y_n are the x and y coordinates, respectively, of the center of the n^{th} cell; and $H_0(k\rho)$ and $H_1(k\rho)$ are respectively the zeroeth- and first-order Hankel functions of the second kind.

The 2N equations represented by Eqs. (B-2) and (B-3) are then solved by a digital computer to give the fields E_{xn} and E_{yn} within the individual cells. Having determined the field inside the cylinder, one may proceed to calculate the scattered field outside the cylinder. The scattered fields are given by:

$$E_x^s(x,y) = \sum_{n=1}^{N} K_n \Big[\{k\rho_n (y - y_n)^2 H_0(k\rho_n) + [(x - x_n)^2 - (y - y_n)^2]$$

$$\cdot H_1(k\rho_n)\} J_{xn} + (x - x_n)(y - y_n)$$

$$\cdot \{2H_1(k\rho_n) - k\rho_n H_0(k\rho_n)\} J_{yn} \Big], \qquad \text{(B-11)}$$

and

$$E_y^s(x,y) = \sum_{n=1}^{N} K_n \Big[(x - x_n)(y - y_n)\{2H_1(k\rho_n) - k\rho_n H_0(k\rho_n)\} J_{xn}$$

$$+ \{k\rho_n (x - x_n)^2 H_0(k\rho_n) + [(y - y_n)^2 - (x - x_n)^2]\, H_1(k\rho_n)\} J_{yn} \Big] \qquad \text{(B-12)}$$

where

$$K_n = - \frac{\pi a_n J_1(ka_n)}{2\omega\varepsilon_1\varepsilon_0\rho_n^3}, \qquad \text{(B-13)}$$

$$\rho_n = \sqrt{(x - x_n)^2 + (y - y_n)^2}. \qquad \text{(B-14)}$$

J_{xn} and J_{yn} are equivalent electric current densities given by:

$$J_{xn} = j\omega\varepsilon_1\varepsilon_0(\varepsilon_n - 1)E_{xn}, \qquad \text{(B-15)}$$

$$J_{yn} = j\omega\varepsilon_1\varepsilon_0(\varepsilon_n - 1)E_{yn}; \qquad \text{(B-16)}$$

ε_1 is the relative dielectric constant of the ambient medium, and $\varepsilon_0 = 8.854 \times 10^{-12}$ F/m, the dielectric constant of free space. The total field external to the cylinder is just the sum of the scattered and incident fields. That is:

$$\underline{E}(x,y) = \underline{E}^i(x,y) + \underline{E}^s(x,y). \qquad \text{(B-17)}$$

For dielectric cylinders or dissipative ambient media, simply substitute for ε_n or ε_1:

$$\varepsilon_1 = \varepsilon_1^r - j\sigma_1/\omega\varepsilon_0, \qquad \text{(B-18)}$$

$$\varepsilon_n = (\varepsilon_n^r - j\sigma_n/\omega\varepsilon_0)/\varepsilon_1, \qquad \text{(B-19)}$$

where ε_1^r and ε_n^r are the real parts of the dielectric constants, and σ_1 and σ_n are conductivities. Also, the k-vector becomes:

$$k = \frac{2\pi}{\lambda} = \frac{\omega}{c} (\varepsilon_1)^{1/2} , \qquad \text{(B-20)}$$

where $c = 3 \times 10^8$ m/s, the velocity of light in free space.